Using graphdiyne (GDY) as a catalyst support for enhanced performance in organic pollutant degradation and hydrogen production: a review

Biao Song[a,b], Ming Chen[a,b], Guangming Zeng[a,b,*], Jilai Gong[a,b,*], Maocai Shen[a,b], Weiping Xiong[a,b], Chengyun Zhou[a,b], Xiang Tang[a,b], Yang Yang[a,b], Wenjun Wang[a,b]

[a] College of Environmental Science and Engineering, Hunan University, Changsha 410082, PR China

[b] Key Laboratory of Environmental Biology and Pollution Control (Hunan University), Ministry of Education, Changsha 410082, PR China

* Corresponding authors at College of Environmental Science and Engineering, Hunan University, Changsha 410082, P.R.China.

Tel: +86 731 88822754; Fax: +86 731 88823701.

E-mail addresses: gzeng@hnu.edu.cn (G. Zeng); jilaigong@hnu.edu.cn (J. Gong)

Abstract

The development of carbon materials brings a new two-dimensional catalyst support, graphdiyne (GDY), which is attracting increasing interest in the field of catalysis. This article presents a systematical review of recent studies about the characteristics, design strategies, and applications of GDY-supported catalysts. The sp- and sp^2-hybridized carbon, high electrical conductivity, direct band gap, and high intrinsic carrier mobility are key characteristics for GDY to serve as a competitive catalyst support. Hydrothermal method (or solvothermal method), GDY in-situ growth, and electrochemical deposition are commonly used to load catalysts on GDY support. In the applications of GDY-supported photocatalysts, GDY mainly serves as an electron or hole transfer material. For the electrocatalytic hydrogen production, the unique electronic structure and high electrical conductivity of GDY can promote the electron transfer and water splitting kinetics. This review is expected to provide meaningful insight and guidance for the design of GDY-supported catalysts and their applications.

Keywords: Graphdiyne; Photocatalyst; Electrocatalyst; Organic pollutant degradation; Hydrogen production

Contents

Abbreviations:

2D, two-dimensional; 3D, three-dimensional; CNT, carbon nanotube; CV, cyclic voltammetry; CVD, chemical vapor deposition; DFT, density functional theory; DMF, dimethyl formamide; DMSO, dimethyl sulfoxide; EIS, electrochemical impedance spectroscopy; g-C_3N_4, graphitic carbon nitride; GDY, graphdiyne; GO, graphene oxide; GR, graphene; HEB, hexaethynylbenzene; HER, hydrogen evolution reaction; LDH, layered double hydroxide; MB, methylene blue; MO, methyl orange; NMP, N-methyl pyrrolidone; NPs, nanoparticles; RhB, rhodamine B; RHE, reversible hydrogen electrode; SCE, saturated calomel electrode; TEOA, triethanolamine; TOF, turnover frequency

1. Introduction

Energy crisis and environmental pollution are two significant issues faced by the humankind nowadays (Alharbi et al., 2018; Musa et al., 2018; Landrigan et al., 2019; Poudyal et al., 2019). The utilization of coal, petroleum, and natural gas has greatly pushed the development process of world economy and human society, and these fossil fuels are the main sources of world energy supply (Nehring, 2009). However, it is estimated that the reserve depletion time of coal, petroleum, and natural gas is only about 107, 35, and 37 years, respectively (Shafiee and Topal, 2009). Thus, the development of renewable energy sources is urgently needed. Hydrogen energy is a widely acknowledged clean energy without carbon emission and has been considered as one of the most promising alternative energy sources (Stern, 2018; Maggio et al., 2019). Producing hydrogen via water splitting is an attractive strategy and many efforts have been made to achieve this goal (Iqbal and Siddique, 2018; Qi et al., 2018; Saraswat et al., 2018; Hisatomi and Domen, 2019; Zhou et al., 2020). On the other hand, numerous pollutants resulted from human activities are discharged into the atmosphere, water, and soil, which threatens human health and reduces life quality. For example, fiber production in textile industry may produce highly contaminated wastewater that contains dyes (e.g., azo, anthraquinone, indigo, triarylmethane, phthalocyanine, and sulphur dyes), heavy metals, acid or alkali, fibers, detergents, sulfides, and nitro compounds (Yaseen and Scholz, 2019). These pollutants may not only cause direct damage to water sources and threaten drinking water safety, but also affect agricultural irrigation and fishery production (Lu et al., 2015; Saha et al., 2017;

Salgot and Folch, 2018). Thus, treating the wastewater is necessary to minimize its harmful effects.

Catalysts play important roles in efficient hydrogen production and organic pollutant degradation. Due to the high catalytic activities, noble metal catalysts, such as Pt, Pd, Ag, and Rh, dominate the current commercial catalyst market (Parmon et al., 2010). However, the resource scarcity, exorbitant price, and relatively low stability of noble metal catalysts limit their large-scale use, which leads to the development of many alternative catalytic materials, such as metal oxides (Smestad and Steinfeld, 2012; Dong et al., 2015), transition metal sulfides (Ivanovskaya et al., 2013; Wu et al., 2017), metal-organic frameworks (Dhakshinamoorthy et al., 2012; Xiong et al., 2018), Mxenes (Gao et al., 2017; Yang et al., 2019a), and many metal-free catalysts (Liu and Dai, 2016; Wang et al., 2019). The development of carbon materials brings many excellent carbon-based catalysts, including carbon nanotube (CNT) (Yan et al., 2015; Song et al., 2018), graphene (GR) (Huang et al., 2012; Liu et al., 2019b), biochar (Lee et al., 2017; Ye et al., 2019), and graphitic carbon nitride (g-C_3N_4) (Naseri et al., 2017; Yang et al., 2019b). Compared with other catalytic materials, carbon-based catalysts show apparent superiority in stability, durability, and cost (Zhai et al., 2015). This enables them to be potential substitutes for noble metal catalysts. Recently, a new class of two-dimensional (2D) carbon materials, graphynes, attracts increasing attention in catalysis field. Graphynes are all-carbon molecules with a planar network structure that contains both sp- and sp^2-hybridized carbon atoms, and it can be viewed as the replacement of carbon-carbon bonds in graphene by one or more acetylenic

linkages. According to the number of acetylenic linkages for replacing each carbon-carbon bond in graphene, graphynes can be classified into graphyne, graphdiyne (GDY), graphtriyne, and so on (Huang et al., 2018; Gao et al., 2019). As currently the most active member of graphyne family, GDY has many different molecular configurations and the typical ones are known as α-GDY, β-GDY, and γ-GDY (Fig. 1a). The Greek letters indicate the closeness of GDY to the symmetric modifications describing them to that for hexagonal graphene layers, where α-GDY is the closest one to graphene (Belenkov et al., 2015). In the molecular configuration of α-GDY, diacetylenic linkages (−C≡C−C≡C−) replace all the carbon-carbon bonds of graphene in the symmetric modification. When only two thirds or one third of the carbon-carbon bonds are replaced by diacetylenic linkages, the resulting GDY is called β-GDY or γ-GDY, respectively. Among these types of GDY, γ-GDY has more stable configuration, and has been mostly studied at present. In this paper, GDY refers to γ-GDY unless otherwise specified. Since the successful synthesis of γ-GDY was reported by Li et al. (2010), GDY has become a research hotspot in materials, chemistry, physics, and energy (Fig. 1b). In the field of catalysis, GDY has been studied as direct catalysts, especially GDY-based metal-free catalysts (Zuo et al., 2019). The sp- and sp^2-hybridized carbon atoms in GDY provide superior electrical and optical properties for catalytic applications (Li et al., 2014). At room temperature, GDY has a direct band gap of 0.46 eV and a high intrinsic carrier mobility of 10^4–10^5 $cm^2\ V^{-1}\ s^{-1}$ (Long et al., 2011; Gao et al., 2019). According to the calculations of density functional theory (DFT), Wu et al. (2014) reported the possibility of GDY as a

134 catalyst for low-temperature CO oxidation via a Eley-Rideal mechanism, in which CO
135 directly react with adsorbed and activated O_2 on the GDY sheet. Many experimental
136 studies demonstrated that nitrogen-doped GDY could be high-performance metal-free
137 catalysts for oxygen reduction reaction (Liu et al., 2014; Lv et al., 2017; Shang et al.,
138 2018; Zhao et al., 2018b). For example, Liu et al. (2014) synthesized nitrogen-doped
139 GDY and applied it for catalyzing oxygen reduction reaction in alkaline fuel cells.
140 Their results suggested comparable electrocatalytic activity of nitrogen-doped GDY to
141 that of commercial Pt/C catalyst.

142 In addition to using GDY as direct catalysts, more studies explored the potential
143 of GDY as a catalyst support. The main roles of catalyst support include increasing
144 the stability and durability of catalyst in severe conditions, making catalyst easy to
145 recycle, improving the adsorption of substrate, and producing a synergistic catalytic
146 effect (Wang et al., 2014; Molnár and Papp, 2017). Even noble metal catalysts with a
147 high catalytic activity need a proper support to enable their large-scale commercial
148 applications. For example, the Pt catalyst is generally available as commercial Pt/C
149 catalyst, using carbon black as a support (Kim et al., 2006). The unique structure of
150 GDY makes it to be an excellent support for not only constructing heterojunction with
151 traditional catalysts but also anchoring atomic catalysts (Huang et al., 2018; Sun et al.,
152 2019). Many excellent and interesting research articles about using GDY as a catalyst
153 support were published in recent years, especially in the applications for organic
154 pollutant degradation and hydrogen production via water splitting. However, to our
155 knowledge, systematic review on this topic has not been reported previously. In this

article, recent studies about GDY-supported photocatalysts and electrocatalysts are carefully reviewed. The main advantages of GDY as a catalyst support are discussed from the points of structure, optics, and electricity. Based on the latest experimental achievements, the strategies for loading catalysts on GDY support are summarized and analyzed. The performance and mechanisms of GDY-supported catalysts in organic pollutant degradation and hydrogen production via water splitting are reviewed and discussed. Some challenges for further developing the catalytic technology with GDY as the catalyst support are presented. This work may help the design of GDY-supported catalysts and their applications.

2. Advantages of 2D GDY as a catalyst support

An ideal catalyst support should have a large surface area, high electrical conductivity, and strong cohesion to catalyst particles. Additionally, considering the application of catalyst in various reactions, the catalyst support should have a porous structure to enable efficient mass transfer, and good resistance to the corrosion from severe reaction conditions. GDY meets these demands in many ways (Fig. 2). In this section, the properties and advantages of GDY in its use as a catalyst support were summarized and discussed.

Compared with GR, GDY has a lower atom density resulting from the 18-C triangular ring structure, which provides a large specific surface area for loading catalyst (Huang et al., 2015). The theoretical specific surface area of GDY is estimated to over 2630 $m^2 g^{-1}$ for GR (Lv et al., 2018; He et al., 2019). In reality, due

178 to the restacking of GR sheets caused by the van der Waals forces, the specific surface
179 area of GR is generally measured at several hundred $m^2\ g^{-1}$ (Ding et al., 2010; Geng
180 et al., 2011). Huang et al. (2015) measured the specific surface area of their
181 synthesized GDY by N_2-adsorption/desorption experiments, and the highest value
182 reached 1329 $m^2\ g^{-1}$. The large surface area is beneficial to the uniform distribution of
183 catalyst particles on GDY sheets, which may reduce the loss of catalytic activity
184 resulting from the aggregation of particles.

185 The sp- and sp^2-hybridized carbon networks with a highly conjugated π-system
186 endow GDY with a high electrical conductivity of 2.516×10^{-4} S m^{-1} at room
187 temperature (Li et al., 2010). Such a conductivity is similar to silicon, indicating the
188 semiconductor feature of GDY. According to the DFT calculations, the GDY sheet has
189 a direct band gap of 0.46 eV, and the intrinsic electron (e^-) mobility and hole (h^+)
190 mobility are 2×10^5 and 2×10^4 $cm^2\ V^{-1}\ s^{-1}$, respectively (Long et al., 2011). These
191 characteristics make GDY superior in improving the electron transport efficiency in
192 catalytic applications, especially in photocatalytic and photoelectrocatalytic reactions.
193 For example, based on the high electrical conductivity and narrow band gap of GDY,
194 Wang et al. (2012) fabricated GDY-supported TiO_2 nanocomposite and applied it for
195 photocatalytic degradation of methylene blue (MB). Their results showed that GDY
196 effectively improved the light absorption of TiO_2 and the separation efficiency of
197 photoinduced electron-hole pairs, thus increasing the photocatalytic activity.

198 The GDY surface can provide strong cohesion to many metal atoms via
199 chemisorption. The study about the interactions between heavy metal atoms and GDY

showed that Ag and Cu atoms could be adsorbed onto the GDY surface via strong chemisorption, rather than typical physisorption between the metal atoms and GR (Mashhadzadeh et al., 2016). Lu et al. (2016) studied the adsorption of noble metal atoms (Pd, Pt, Rh and Ir) on GDY surface by theoretical calculation, and found that these noble metal atoms could be embedded in the 18-C alkyne ring of GDY. For single metal atoms, the most favorable adsorption site on GDY is at the angle site of the alkyne ring (Yu et al., 2019). The sp hybridization of acetylene bond in GDY enables the π/π^* orbitals to rotate towards any direction perpendicular to the line of −C≡C−, and thus it can point to a metal atom (He et al., 2012). These properties make GDY a promising support for metal atomic catalysts that have high atomic efficiency, catalytic activity, and selectivity.

The big triangular rings of GDY offer a porous structure for fast mass transfer and more exposed active sites. In GDY-supported catalysts, the diffusion of substrate and product can be achieved not only along the GDY layer plane, but also through the 18-C triangular pores. This characteristic is especially beneficial for bulk GDY with multilayer structure. Zhang et al. (2013) conducted a first-principles study about the three-dimensional (3D) diffusion of H_2 molecules in GDY, and found that the out-plane diffusion of H_2 molecules through the large triangular pores in GDY had an easily surmountable energy barrier of ∼0.16 eV. This result indicates that the porous structure allows 3D diffusion (in-plane and out-plane diffusion) of H_2 in GDY, which is more favorable to the mass transfer than that in graphite where the diffusion of H_2 is limited to in-plane diffusion in the interlayer space.

GDY has shown excellent chemical stability in organic solvents and strongly acidic/alkaline solutions (Li et al., 2019a). During the catalytic process, many catalyst supports suffer from severe corrosion that may significantly influence the stability of supported catalysts. Benefiting from the 2D structure of sp- and sp^2-hybridized carbon atoms, GDY has been predicted to be the most stable diacetylenic carbon allotrope (Li et al., 2010). Xue et al. (2016) synthesized an electrocatalyst of GDY-supported Co nanoparticles (NPs) wrapped by N-doped carbon, and reported that this catalyst has extraordinary durability at all pH values in its application for hydrogen production. According to their measurement, the catalytic activity of commercial Pt/C (10 wt%) significantly decreased after only 8000 cycles of continuous cyclic voltammetry (CV) scanning (at all pH values), while the high catalytic activity of the GDY-supported electrocatalyst could be kept over 36000, 28000, and 9000 cycles under alkaline, acidic, and neutral conditions, respectively. This result demonstrates that GDY has good resistance to the corrosion from severe reaction conditions and the GDY-supported catalysts can be more stable and more durable than common commercial catalysts.

3. Design of 2D GDY-supported catalysts

3.1. Synthesis of GDY

Though the structure of GDY has been theoretically predicted before (Haley et al., 1997), it was not until 2010 that Prof. Yuliang Li and his coworkers (Li et al., 2010) first synthesized GDY via an in-situ cross-coupling reaction of

hexaethynylbenzene (HEB) monomers on a Cu foil (Fig. 3a). In the synthesis process, pyridine is used as both ligand and solvent, and Cu foil is used as both catalyst and substrate for the directional polymerization of GDY film. In the presence of pyridine, Cu^{2+} can be gently produced from the Cu foil and catalyze the coupling reaction. Such a Cu-catalyzed terminal alkyne coupling reaction is a typical Glaser-Hay coupling reaction, in which the dioxygen activation of two molecules of Cu-acetylide is considered the key step of the reaction mechanism (Fig. 3b) (Fomina et al., 2002).

Since the first successful synthesis of GDY was reported, many more methods have been proposed and used to synthesize GDY and its derivatives. As some side reactions with the reactive HEB monomers and irregular cross-linking between two acetylenic linkages may occur, it is still a challenge to produce high-quality graphdiyne films. Therefore, choosing a flat substrate that can properly interact with the precursor is important to obtain the desired 2D structure, and supramolecular interactions may be utilized as an additional strategy to control the orientation of precursor and product (Zhou et al., 2019).

Considering the bulk polymerization of HEB in the original method due to the diffusion of Cu^{2+} catalyst, Matsuoka et al. (2017) reported a GDY synthesis method at a liquid/liquid or gas/liquid interface to obtain a thin GDY nanosheet. For synthesizing GDY at a liquid/liquid interface, immiscible dichloromethane and water were used (Fig. 4a). The HEB monomer was included in the lower dichloromethane layer, while the upper aqueous layer contained $Cu(OAc)_2$ and pyridine. Before the addition of the upper aqueous layer, the dichloromethane layer was first covered with

pure water to keep the interface still when the upper aqueous solution was added. This operation could avoid the random contact of catalyst and HEB and ensure the high quality of resulting GDY nanosheet. For synthesizing GDY at a gas/liquid interface, an aqueous solution containing $Cu(OAc)_2$ and pyridine was used as the liquid phase (Fig. 4b). A small amount of dichloromethane and toluene mixture containing HEB was added to the surface of the aqueous solution under an argon atmosphere. Quick evaporation of the organic solvent enabled the smooth catalytic polymerization at the gas/liquid interface. The product could be transferred to a flat substrate by bringing the substrate close to the interface in the horizontal direction. According to the reported results, the thickness of GDY sheet synthesized at the gas/liquid interface (3 nm) was thinner than that synthesized at the liquid/liquid interface (24 nm). The GDY product prepared by interfacial synthesis method is of thin layer and high crystallinity, and suitable for studying the intrinsic properties of GDY.

Liu et al. (2017) proposed a chemical vapor deposition (CVD) method for GDY growth on a silver foil (Fig. 4c). In the CVD system, the precursor HEB was placed upstream and transported by carrier gas to the Ag foil surface. The coupling reaction occurred at 150 ℃. Through thermal activation and Ag catalysis, the monomers were coupled and formed GDY sheet. In the synthesis process, the growth of GDY was self-limited as the catalyst would not be available for further coupling reaction once the Ag foil surface was completely overlaid. Such a process was confirmed by the characterization result that the synthesized GDY had a uniform monolayer structure (0.6 nm). The GDY product synthesized by CVD method is thinner than that prepared

by the interfacial synthesis method, but the film is noncrystalline.

Zuo et al. (2017) reported a facile explosion approach for GDY synthesis without metal catalyst (Fig. 4d). In their scheme, the coupling reaction was performed by directly heating HEB in N_2 or air with different heating rates. The obtained GDY products exhibited different morphology, including nanoribbon, 3D framework, and nanochain. When the precursor HEB in light yellow was gradually heated to 120 ℃ in N_2, nanoribbon GDY in dark black was formed without volume change. When the heating treatment was conducted in air, a popcorn-like explosion occurred and 3D framework GDY was produced with a sixfold volume increase. Particularly, the explosion became more violent when the precursor was directly added to pre-heated air at 120 ℃, and the resulting GDY showed a nanochain morphology. This explosion approach is fast for large-scale preparation of GDY from HEB in air, and no use of metal catalyst can avoid unnecessary contamination.

3.2. Loading catalysts on GDY support

As a new 2D carbon-based support, GDY shows promising application prospects in constructing various heterojunction catalysts with other 0D, 1D, and 2D materials. Many strategies have been proposed and used for effectively loading catalysts on GDY support (Table 1). In this section, the basic principles and applications of these strategies are presented and discussed in detail.

3.2.1. Hydrothermal method (or solvothermal method)

Hydrothermal method (or solvothermal method) is the most widely used method for loading catalysts on GDY support. This method is based on the chemical reactions that occurred in a sealed pressure vessel under high-temperature and high-pressure conditions, with water (or organic solvents) as the reaction medium (Feng and Li, 2017; Song et al., 2019). Pre-prepared catalysts can be directly loaded on GDY support by hydrothermal method (or solvothermal method) via combination reactions. For example, Wang et al. (2012) synthesized GDY-supported TiO_2 NPs by hydrothermal combination of pre-prepared GDY sheets and purchased TiO_2 NPs, and the spectral analyses suggested that the TiO_2 NPs combined with the active sites of GDY sheets by forming Ti−O−C bonds, rather than simple physical mixing. In order to obtain metal-free catalysts, Han et al. (2018) immersed GDY nanosheet array into a dispersion of g-C_3N_4 in NMP and conducted a solvothermal reaction. Their results showed that g-C_3N_4 and GDY successfully combined through the π-π stacking interaction, but this interaction was not observed in the physical mixture of g-C_3N_4 and GDY at room temperature.

Apart from combination reactions, hydrothermal (or solvothermal) crystallization is a more general mechanism for loading catalysts on GDY support. In such a loading process, catalyst precursors are dissolved in the thermal medium under high-temperature and high-pressure conditions, and GDY induces the heterogeneous nucleation and crystal growth of catalyst. Lv et al. (2019) prepared a CdS/GDY photocatalyst by the hydrothermal method. In their experiments, $Cd(OAc)_2$ was added

into the DMSO dispersion of GDY, and the DMSO acted as both solvent and sulfur source. After the hydrothermal reaction at 180 ℃ for 12 h, uniform distribution of CdS NPs on the GDY surface was observed by electron microscope images. Kuang et al. (2018) fabricated a Ni-Fe-LDH/GDY electrocatalyst by hydrothermal method. According to their illustration (Fig. 5), the metal ions could be chemically adsorbed by the π-bond of GDY acetylenic bond at the initial stage of hydrothermal reaction, and then in-situ crystal growth of Ni-Fe-LDH occurred on the GDY surface as the reaction progressed. The GDY acetylenic bond consists of two π-bonds and one σ-bond. Generally, the π-bond is active and it can coordinate with transition metal atoms by donating electron to the metal empty orbitals (Liu et al., 2019a). Additionally, it was noticed that the combination way of GDY and Ni-Fe-LDH was not face-to-face, but face-to-side (Fig. 5). Such a 3D structure provided more active sites for catalytic reactions. Using hydrothermal method (or solvothermal method) to load catalysts on GDY support is effective and easy to implement in general laboratories.

3.2.2. GDY in-situ growth

Inspired by the synthesis method of GDY, the combination of GDY and other catalysts can be achieved during the synthesis process of GDY by using the catalyst as the GDY growth substrate instead of Cu foil. This is a reverse loading method, in which the loaded catalyst is prepared first and then the GDY grows in situ on the catalyst surface. On this account, the in-situ growth method is mainly used for

353 assembling GDY with some 2D catalyst materials, such as LDH (Fang et al., 2019),
354 MoS_2 (Hui et al., 2019b), and GR (Li et al., 2019b). The direct growth of GDY on
355 catalyst substrate can reduce the resistance of charge transfer across the heterojunction
356 interface, which is conducive to the improvement of catalytic reaction rate (Fang et al.,
357 2019). Additionally, the tightly adhered GDY can provide a protective effect on the
358 catalyst and enhance its durability (Hui et al., 2019a).

359 Fang et al. (2019) synthesized a CoN_x/GDY electrocatalyst through the GDY
360 in-situ growth method (Fig. 6). In their experiment, a Co-LDH on Ni foam was first
361 prepared by a hydrothermal reaction, with the foam color changing from silver to
362 saddlebrown. Then, the obtained Co-LDH underwent a nitridation treatment to form
363 CoN_x, and the foam color further changed to green yellow. Finally, olive CoN_x/GDY
364 on Ni foam was synthesized by the cross-coupling reaction of HEB monomers on the
365 CoN_x surface. Similarly, Hui et al. (2019a) first synthesized iron carbonate hydroxide
366 nanosheets on Ni foam, and then used the nanosheets as the substrate for in-situ
367 growth of GDY to obtain an electrocatalyst for water splitting. Due to the protective
368 effect of GDY, the electrocatalyst exhibited excellent long-term durability in the
369 subsequent electrochemical tests. They further used MoS_2 nanosheet as the substrate
370 for GDY in-situ growth, and found that strong electron hybridization was formed due
371 to the chemisorption of active GDY by MoS_2, thus improving the electrical
372 conductivity and catalytic activity of MoS_2/GDY electrocatalyst (Hui et al., 2019b).
373 Additionally, the MoS_2/GDY electrocatalyst showed excellent stability at all pH
374 values when being used as an efficient cathode for hydrogen generation. Li et al.

(2019b) used GR as the substrate for GDY in-situ growth. According to their results, GDY grew on both sides of GR sheets due to the van der Waals interaction and lattice match between GDY and GR. These studies provide valuable information for combination 2D catalysts with GDY support by GDY in-situ growth.

3.2.3. Electrochemical deposition

Electrochemical deposition is a convenient method for depositing metals, alloys, or composite coatings on the surface of conductive substrate to obtain the desired surface characteristics, and this method has been widely used for the synthesis of composite materials (Góral et al., 2017; Zhao et al., 2018a; Qiao et al., 2019). Some studies reported the use of electrochemical deposition to load catalysts on GDY support. Generally, GDY is used as the working electrode and immersed in an electrolyte solution containing metal catalyst precursors. Under an external electric field, metal ions migrate to the electrode, and deposit on the GDY surface through redox reactions. Shi et al. (2019) prepared Ni-Fe-LDH/GDY electrocatalyst by the electrochemical deposition of Ni-Fe-LDH on GDY surface. The synthesis process was conducted in a three-electrode system, in which Cu foil overlaid with GDY, Pt foil, and saturated calomel electrode (SCE) were used as working electrode, counter electrode, and reference electrode, respectively. The electrolyte solution was prepared by dissolving $Ni(NO_3)_2$ and $FeSO_4$ in deionized water. The deposition process lasted for 90 s with a constant potential of −1.0 V (vs. SCE). Hydroxide ions (OH^-) needed for forming Ni-Fe-LDH were provided by the reduction of NO_3^- at the working

electrode (Eq. (1)) (Yarger et al., 2008).

$$NO_3^- + H_2O + 2e^- \rightarrow NO_2^- + 2OH^- \quad (1)$$

Electrochemical deposition method is more typically used for loading metal atomic catalysts on GDY sheet. Xue et al. (2018) anchored Ni and Fe atoms on GDY growing on 3D carbon cloth by electrochemical deposition (Fig. 7). In their experiments, GDY was first prepared on a 3D carbon cloth by the Glaser-Hay coupling reaction. Then, the GDY was immersed in an electrolyte solution containing Ni^{2+} or Fe^{3+}, allowing the adsorption of metal ions on GDY. The deposition of Ni and Fe atoms on GDY surface was achieved by in-situ electrochemical reduction of the metal ions. The electrochemical deposition was performed with a constant current density of 10 mA cm^{-2}, and the deposition time was 150 s and 250 s for Ni and Fe, respectively. In the electrochemical deposition process, the strict control of metal ion concentration and deposition time is the key to obtain well-separated atom catalysts on GDY sheet. Yu et al. (2019) synthesized Pd^0/GDY electrocatalyst by electrochemical deposition of Pd atoms on GDY in a three-electrode system. The electrochemical deposition was conducted at a current density of 2 mA cm^{-2} for 10 s after immersing the GDY electrode into 0.2 mM $PdCl_2$ solution. The same deposition process resulted in a Pd NPs/GDY product when the $PdCl_2$ concentration was 1.0 mM and the deposition time lasted for 100 s. Electrochemical deposition is a fast and efficient method to load catalysts on GDY support, and the loading amount of catalysts can be well controlled through adjusting the concentration of catalyst precursor in electrolyte solution and the deposition time.

3.2.4. Others

In addition to the above methods, oil-in-water microemulsion method, calcination method, sequential annealing treatments, and microwave-assisted reduction were tried to loading catalysts on GDY sheet. Zhang et al. (2015) loaded Ag/AgBr on GDY sheet by oil-in-water microemulsion method, with the assistant of graphene oxide (GO) as a cross-linking agent. In their experiments, GDY sheets were first added into the aqueous suspension of GO, followed by ultrasonic treatment to obtain homogeneous GO-GDY dispersion. Then, the GO-GDY dispersion was added into an aqueous solution of $AgNO_3$. After sufficient stirring, a chloroform solution of CTAB was added dropwise. The Ag/AgBr/GO/GDY product was collected and washed by repeated centrifugalization after the evaporation of chloroform. In such a synthesis process, the Ag/AgBr nucleated and grew in the microvesicle of microemulsion, which contributed to the formation of well-dispersed and even-sized Ag/AgBr on the GDY surface. Considering the high temperature resistance of GDY, Xu et al. (2019) used a calcination method to synthesize g-C_3N_4/GDY photocatalyst. The g-C_3N_4 and GDY were pre-prepared by thermal polymerization and cross-coupling reaction, respectively. Homogenous GDY suspension (in methanol solution) and g-C_3N_4 suspension (in aqueous solution) were then obtained with ultrasonic treatment. After thoroughly mixing the two suspensions, the solvents were removed and the resulting solid was thermally treated at 400 °C for 2 h to produce g-C_3N_4/GDY composite. According to their characterization results, g-C_3N_4 and GDY

were firmly connected by the new C−N bond formed between them. A similar experiment was performed by Xue et al. (2016) to load Co NPs wrapped by N-doped carbon on GDY sheet, but the thermal treatment is a sequential annealing process (500 ℃ for 2 h, and 700 ℃ for 2 h) in Ar atmosphere. Before the thermal treatment, the GDY was mixed with cobalt acetate and dicyandiamide rather than pre-prepared catalyst. The product was obtained after the thermal treatment and an additional acid treatment with 0.5 M H_2SO_4. Shen et al. (2019) reported a microwave-assisted reduction method for loading Pt NPs on GDY sheet. In their experiments, chloroplatinic acid (H_2PtCl_6) solution was used as the Pt source and mixed with an ethylene glycol dispersion of GDY. After ultrasonic treatment for 30 min, the mixture was transferred to quartz tubes placed in a microwave equipment (400 W). The reduction reaction was conducted at 160 ℃ for 2 min to produce Pt NPs/GDY composite. With the assistance of microwave, the synthesis process was time-saving and the produced Pt NPs showed small particle sizes (2–3 nm).

4. Applications of GDY-supported catalysts

The catalysts supported by GDY show promising applications in efficient hydrogen production from water splitting and effective degradation of organic pollutants (Table 2). In this section, the performances and mechanisms of GDY-supported catalysts (including photocatalysts and electrocatalysts) are reviewed and discussed, and the discussion mainly focuses on how GDY functions in these catalytic applications.

463

464 *4.1. GDY-supported photocatalysts for organic pollutant degradation*

465 Photocatalytic technology is promising for treating organic wastewater,
466 especially those containing refractory organics that cannot be removed by traditional
467 biological treatment processes (Teixeira et al., 2016; Xu et al., 2017; Liu et al., 2019c).
468 Photocatalytic degradation of organic pollutants is energy-saving, as it can utilize
469 solar energy to drive the photochemical reactions (Zhang and Lou, 2019). Using
470 GDY-supported photocatalysts can effectively promote the degradation efficiency.
471 Dong et al. (2018) reported enhanced photocatalytic activity in degrading RhB by
472 N-doped TiO_2/GDY under visible light irradiation. With the assistance of GDY, the
473 degradation efficiency increased from 78% to about 90% within 240 min (Fig. 8a).
474 For investigating the main reactive species that contributed to the RhB degradation,
475 the authors performed the photocatalytic degradation experiments with N-doped
476 TiO_2/GDY in the presence of different scavengers, including N_2 for $\cdot O_2^-$, isopropanol
477 (IPA) for $\cdot OH$, and triethanolamine (TEOA) for h^+. The addition of N_2 and TEOA
478 significantly inhibited the RhB degradation (Fig. 8b), which suggested the important
479 roles of $\cdot O_2^-$ and h^+ in the photocatalytic degradation of RhB. According to the
480 proposed degradation mechanism (Fig. 8c), the visible light irradiation could excite
481 electrons from the valance band (VB) to the conduction band (CB) of TiO_2, leaving
482 holes in the VB. Because of the more negative CB potential of TiO_2 (−0.47 eV) than
483 the Fermi level of GDY (−0.33 eV) and the high electrical conductivity of GDY, the
484 electrons in the CB of TiO_2 could move to GDY and transfer along the GDY surface.

The adsorbed O_2 on GDY then accepted the electrons and formed O_2^-. Both h^+ and O_2^- are strong oxidants, which resulted in the oxidative degradation of RhB. The electron transfer effect of GDY was also reported in the photocatalytic applications of TiO_2/GDY (Wang et al., 2012; Yang et al., 2013), ZnO/GDY (Thangavel et al., 2015), and Ag/AgBr/GO/GDY (Zhang et al., 2015). In these studies, GDY mainly functions by serving as the electron acceptor and reducing the recombination of photoinduced electron-hole pairs, which allows more holes to participate in the oxidation of organic pollutants. Additionally, the transferred electrons by GDY might react with oxygen molecules and form reactive oxygen species, playing an indirect role in the photocatalytic degradation of organic pollutants.

Additionally, Wang et al. (2012) reported that GDY could modify the bandgap of TiO_2 and expand its light absorption range. Based on the band structure calculations of TiO_2/GDY and the photocatalytic experiments, the authors considered that the introduction of C-2p impurity bands narrowed the bandgap of TiO_2 and increased the visible light absorption, which contributed to the high photocatalytic performance of TiO_2/GDY in degrading MB. The impurity energy level located between VB and CB of TiO_2/GDY is isolated, leading to an easier transfer of electron from VB maximum to impurity energy level or from impurity energy level to CB minimum. At the same time, the electrons are difficult to fall back from CB to VB in the presence of impurity energy level, which impedes the fast recombination of electron-hole pairs (Yang et al., 2013). Zhang et al. (2015) observed more significant enhancement of the photocatalytic activity of Ag/AgBr by the synergistic effect of GDY and GO. Both

GDY and GO could enhance the photocatalytic degradation of MO by Ag/AgBr, and the prepared Ag/AgBr/GO and Ag/AgBr/GDY increased the degradation efficiency from 37.6% to 63.7% and 74.1%, respectively (Fig. 9A). When using Ag/AgBr/GO/GDY as the photocatalyst, almost all of MO was degraded within 40 min, and the degradation rate further increased (Fig. 9A and B). The superior photocatalytic performance of Ag/AgBr/GO/GDY was consistent with its high transient photocurrent response (Fig. 9C). These results were attributed to the effective separation of photoinduced charge carriers and the fast interfacial charge transfer resulting from the synergistic effect of GDY and GO, which was indicated by a smaller semicircular arc in the electrochemical impedance spectra (Fig. 9D). These studies suggested the roles of GDY in modulating the band structure, light absorption capacity, and interfacial charge transfer capacity of GDY-supported photocatalysts.

4.2. GDY-supported photocatalysts for hydrogen production

Hydrogen production from water splitting is expected to ease the current energy crisis. Using GDY-supported photocatalysts can effectively convert solar energy into clean and renewable hydrogen energy. Lv et al. (2019) synthesized various CdS/GDY photocatalysts by using different weight ratio of GDY to $Cd(OAc)_2$ (0.5%, 1%, 2.5%, and 5%, denoted as GD0.5, GD1, GD2.5, and GD5 by the authors, respectively). According to their experimental results, GD2.5 exhibited the highest performance in photocatalytic hydrogen production from water splitting, showing with a hydrogen evolution amount of 4.1 mmol g^{-1} within 10 h (Fig. 10a). For comparison, the authors

studied the hydrogen evolution over time with GD2.5, CdS, and a physical mixture of GDY (2.5%, w/w) and CdS. The results showed that no significant difference was made between the CdS and the physical mixture of GDY and CdS in the hydrogen evolution (Fig. 10b), which indicated that the chemical bonding of GDY and CdS was of crucial importance for the enhanced photocatalytic activity. Different from the photocatalytic oxidative degradation of organic pollutants, the hydrogen evolution is a reduction process, in which H^+ accepted the photoinduced electrons to produce H_2 (Fig. 10c). Thus, the transfer of holes could reduce the recombination of photoinduced charge carriers and create more opportunities for the photoinduced electrons to participate in the reduction process. The high hole mobility in GDY enabled it be to effective hole transfer material for separating photoinduced electron-hole pairs in CdS. The band structure analysis confirmed that the photoinduced holes in the VB of CdS could move to the VB of GDY due to the more positive VB potential of CdS (Fig. 10d). The high intrinsic mobility of electron and hole in GDY makes it effective in helping the supported photocatalysts to improve both oxidizing capacity and reducing capacity.

Xu et al. (2019) fabricated g-C_3N_4/GDY photocatalyst for hydrogen production from water splitting. The g-C_3N_4/GDY containing 0.5% (w/w) GDY contributed to a highest hydrogen evolution rate of 39.6 μmol h^{-1}, which was 6.7 times higher than that by g-C_3N_4 (Fig. 11a). In the photocatalytic experiments, Pt NPs (1%, w/w) were pre-loaded on the photocatalyst surface as a cocatalyst to gather the photoinduced electrons, and TEOA was used as a sacrificial agent to deplete the photoinduced holes.

Because the work function of g-C_3N_4 (4.3 eV) is smaller than that of GDY (5.14 eV), electrons can move from g-C_3N_4 to GDY and form a Schottky barrier. Thus, photoinduced electrons in the CB of g-C_3N_4 moved to GDY and further transfer to the Pt NPs for H^+ reduction in the photocatalytic process (Fig. 11b). It was considered that there were two GDY-assisted electron transfer routes: π-π conjugation and newly formed C−N bonds between g-C_3N_4 and GDY. These two routes for electron transfer and the hole depletion by TEOA promoted the effective separation of photoinduced charge carriers, and thus increased the photocatalytic hydrogen evolution. This example showed the roles of unique electronic characteristics and high electrical conductivity of GDY in enhancing the photocatalytic activity of GDY-supported catalysts.

4.3. GDY-supported electrocatalysts for hydrogen production

Electrocatalytic hydrogen production via water splitting is driven by the electrode potential beyond the equilibrium potential (overpotential), and the hydrogen evolution reaction (HER) occurs at the interface between cathode and electrolyte (Zhou et al., 2016). Using electrocatalysts can reduce the overpotential for overcoming the reaction activation energy and enhance the HER efficiency. Currently, Pt-based electrocatalysts are mainly used for HER because of the excellent performance. However, the low reserve of Pt on Earth cannot meet the high electrocatalyst demand for HER at a large industrial scale (Zhang et al., 2019). The GDY-supported electrocatalysts are promising candidates for high-performance HER.

573 Xue et al. (2018) synthesized Ni^0/GDY and Fe^0/GDY electrocatalysts and used them
574 for HER. Both Ni^0/GDY and Fe^0/GDY showed high catalytic activity for hydrogen
575 evolution. As shown in Fig. 12a, current density at the two catalyst electrodes
576 increased rapidly with the increasing overpotential. Fe^0/GDY exhibited the highest
577 catalytic activity, and its onset overpotential was 9 mV, close to that of Pt/C (20 wt%,
578 1.0 mV). For assessing the catalytic performance more straightforward, the authors
579 calculated the mass activity of Ni^0/GDY, Fe^0/GDY, and Pt/C based on the
580 normalization of loaded metal. Both Ni^0/GDY and Fe^0/GDY exhibited higher mass
581 activity than that of Pt/C (Fig. 12b). For example, at the overpotential of 50 mV, the
582 mass activity of Ni^0/GDY, Fe^0/GDY, and Pt/C was 1.26, 3.52, and 0.12 A mg^{-1},
583 respectively. Compared with some state-of-the-art HER electrocatalysts, Ni^0/GDY,
584 Fe^0/GDY showed higher turnover frequency (TOF, Fig. 12c), which is defined as the
585 turnover number of reactants converted into target products per unit of catalytic
586 activity site in unit time. For the HER mechanism, three possible elementary reactions
587 are involved (Sheng et al., 2013; Morales-Guio et al., 2014):
588 Volmer reaction:
589 $H^+ + e^- \rightarrow H_{ad}$ (acidic condition) (2)
590 $H_2O + e^- \rightarrow H_{ad} + OH^-$ (alkaline condition) (3)
591 Heyrovsky reaction:
592 $H_{ad} + H^+ + e^- \rightarrow H_2$ (acidic condition) (4)
593 $H_{ad} + H_2O + e^- \rightarrow H_2 + OH^-$ (alkaline condition) (5)
594 Tafel reaction:

595 $H_{ad} + H_{ad} \rightarrow H_2$ (6)

596 where H_{ad} represents the adsorbed hydrogen atom at the active site of electrode. The
597 first reaction above is the Volmer or discharge reaction, in which a hydrogen ion or
598 water molecule combines with an electron and forms a hydrogen atom adsorbed on
599 the active site of electrode. After that, H_2 can be formed through the Heyrovsky
600 reaction or the Tafel reaction. In actual experiments, the specific hydrogen evolution
601 route can be inferred from the Tafel slope (Shinagawa et al., 2015). The Tafel slope of
602 Ni^0/GDY, Fe^0/GDY synthesized by Xue et al. (2018) suggested a Volmer-Heyrovsky
603 mechanism for the hydrogen evolution process (Fig. 12d). Additionally, the stability
604 of Ni^0/GDY and Fe^0/GDY electrocatalysts was excellent. As shown in Fig. 12e and f,
605 no loss of the catalytic activity was observed after 5000 cycle tests.

606 Xue et al. (2017) highlighted the roles of GDY in enhancing the electrocatalytic
607 activity of $NiCo_2S_4$ nanowires. The synthesized $NiCo_2S_4$ nanowires/GDY exhibited a
608 much lower onset overpotential for HER (112 mV) than that of the $NiCo_2S_4$
609 nanowires supported by carbon cloth (329 mV). The authors further used the
610 electrochemical impedance spectroscopy (EIS) to analyze the studied electrocatalysts,
611 and fitted the Nyquist plots to an equivalent circuit model (Fig. 13a and b). According
612 to the fitting results, the charge transfer resistance (R_1) of $NiCo_2S_4$ nanowires/GDY
613 was 18.62 Ω, which was much lower than that of carbon cloth (1523 Ω), GDY foam
614 (326.9 Ω), and $NiCo_2S_4$ nanowires/carbon cloth (1476 Ω). This result suggested that
615 using GDY as the support of $NiCo_2S_4$ nanowires was beneficial to increasing the
616 charge transport performance in HER. Due to the electrical conductivity of GDY,

electrocatalysts can directly grow on the GDY support without using polymer binders and other conductive additives, which reduces the charge transfer resistance and contact resistance in electrocatalytic reactions (Fang et al., 2019). Additionally, the synthesized $NiCo_2S_4$ nanowires/GDY showed the highest electrochemical surface area determined by the CV method (Fig. 13c and d). The double layer capacitance of $NiCo_2S_4$ nanowires/GDY was 60 mF cm^{-2}, which was higher than that of carbon cloth (1.0 mF cm^{-2}), GDY foam (1.6 mF cm^{-2}), and $NiCo_2S_4$ nanowires/carbon cloth (21 mF cm^{-2}). Thus, the high electrocatalytic activity of $NiCo_2S_4$ nanowires/GDY could be attributed to the growth of $NiCo_2S_4$ nanowires on GDY support, which increased the electrochemical surface area and active sites for HER.

To further improve the catalytic performance of GDY, doping GDY with heteroatoms (e.g., N, B) was considered an effective strategy as it can modify the electronic structure of GDY. Compared with pristine GDY, N-doped GDY and B-doped GDY improved the catalytic activity due to the electronegativity difference between carbon and hetero atoms (Lv et al., 2017; Zhao et al., 2019). According to the first-principles study, acetylenic linkage sites are the most preferable sites for nitrogen doping (Das et al., 2016). Yu et al. (2018) synthesized MoS_2/N-doped GDY heterostructure and found it suitable as an excellent HER cathode. In the analysis of the HER performance, MoS_2/N-doped GDY showed much higher electrocatalytic activity, more favorable reaction kinetics, and better stability in acidic medium than commercial Pt/C catalysts.

5. Conclusion and outlook

In summary, GDY is an excellent catalyst support for loading various photocatalysts and electrocatalysts. This new 2D carbon-based material has a large specific surface area, high electrical conductivity, direct band gap, high intrinsic carrier mobility, strong cohesion to metal atoms, porous structure, and excellent chemical stability. These properties make GDY as a catalyst support superior to GR and CNT in many ways. Hydrothermal method (or solvothermal method), GDY in-situ growth, and electrochemical deposition are common strategies for effectively loading catalysts on GDY support. In the applications of GDY-supported photocatalysts, GDY mainly serves as electron or hole transfer material to facilitate the charge separation. The transfer of electrons provides more opportunities for the holes to oxidize the organic pollutants, while the transfer of holes allows more electrons to participate in HER. In the applications of GDY-supported electrocatalysts for hydrogen production, the unique electronic characteristics and high electrical conductivity of GDY can promote the electron transfer and water splitting kinetics. In future research, the following issues might be considered for further developing the catalytic technology with GDY as the catalyst support.

(1) Synthesis method and production facility for controllable mass production of GDY should be developed. Though many methods have been developed for synthesizing GDY in the laboratory, they are still insufficient for commercial mass production. The development of both synthesis method and production facility is required to further improve the product quality and yielding capacity of GDY.

(2) New techniques for more effective characterization of the microstructure and chemical bonds of GDY are needed to understand the interactions between catalysts and GDY support. Progress in this respect might optimize the assembly methods for loading various catalysts on GDY and enhance the structural stability of GDY-supported catalysts.

(3) Although GDY-supported catalysts have shown excellent catalytic activity in various applications, there is still room to achieve better catalytic performance by modulating the electrical and optical properties of GDY. For example, doping other elements and surface modification (via covalent bonding or non-covalent bonding) are both effective strategies to further enhance the catalytic performance.

(4) More research on modulating the shape, size, and layer of GDY should be conducted to meet the requirements of different catalytic systems. For example, apart from 2D GDY-supported photocatalysts, some 3D GDY-like materials have been being designed for photocatalytic hydrogen production, such as dehydrobenzoannulene-based 3D GDY (Shen et al., 2020). Additionally, how different types of GDY affect the catalytic performance of GDY-supported catalysts needs to be illuminated by more experimental studies.

(5) The application of GDY-supported electrocatalysts for organic pollutant degradation may be considered. To our knowledge, no GDY-supported electrocatalysts for organic pollutant degradation have been reported yet. However, electrochemical degradation of organic pollutants has been studied for many years. Using GDY-supported electrocatalysts for organic pollutant degradation is

promising, especially for a small amount of organics with high toxicity.

(6) There is a need to study the catalytic reaction mechanisms in depth. Little is known about the interactions between catalysts, GDY support, and reactant molecules in the catalytic processes. Studying the behaviors of differently hybridized carbons in GDY will be beneficial to understanding the catalytic mechanisms and giving full play to the function of GDY.

(7) As GDY is also very active in its theoretical research, more theoretical studies may be conducted to extend the knowledge about the relationship between electronic structure of GDY and its catalytic performance, as well as the design of GDY-supported catalysts. For example, the molecular adsorption behavior on GDY surface and the doping modification of GDY can be further studied through the first principles method.

(8) Currently, few studies revealed the environmental and health-related concerns of GDY. Several biomedical application studies involved the positive aspects of GDY biosafety (Jin et al., 2018; Liu et al., 2019a). Based on the experience and lessons of CNT, GR, and GO, more toxicity and biocompatibility studies should be conducted on this new carbon support material, especially for its nanoparticle forms in different catalytic systems.

(9) Using GDY as a catalyst support just starts in the recent few years. More GDY-supported catalysts can be designed and developed, especially with some emerging catalytic materials (e.g., metal-organic frameworks). The experience from traditional carbon-based catalyst support (e.g., GR) may be considered for

705 reference, and more creative ideas are expected to be found.

706

Acknowledgements

This work was supported by National Natural Science Foundation of China (51521006, 51579095, 51378190, 51508177), the Program for Changjiang Scholars and Innovative Research Team in University (IRT-13R17), and the Three Gorges Follow-up Research Project (2017HXXY-05).

713 **References**

714 Alharbi, O.M.L., Basheer, A.A., Khattab, R.A., Ali, I., 2018. Health and
715 environmental effects of persistent organic pollutants. Journal of Molecular
716 Liquids 263, 442-453.

717 Belenkov, E.A., Mavrinskii, V.V., Belenkova, T.E., Chernov, V.M., 2015. Structural
718 modifications of graphyne layers consisting of carbon atoms in the sp- and
719 sp^2-hybridized states. Journal of Experimental and Theoretical Physics 120,
720 820-830.

721 Das, B.K., Sen, D., Chattopadhyay, K.K., 2016. Nitrogen doping in acetylene bonded
722 two dimensional carbon crystals: Ab-initio forecast of electrocatalytic activities
723 vis-à-vis boron doping. Carbon 105, 330-339.

724 Dhakshinamoorthy, A., Alvaro, M., Garcia, H., 2012. Commercial metal–organic
725 frameworks as heterogeneous catalysts. Chemical Communications 48,
726 11275-11288.

727 Ding, Y., Jiang, Y., Xu, F., Yin, J., Ren, H., Zhuo, Q., Long, Z., Zhang, P., 2010.
728 Preparation of nano-structured $LiFePO_4$/graphene composites by co-precipitation
729 method. Electrochemistry Communications 12, 10-13.

730 Dong, H., Zeng, G., Tang, L., Fan, C., Zhang, C., He, X., He, Y., 2015. An overview
731 on limitations of TiO_2-based particles for photocatalytic degradation of organic
732 pollutants and the corresponding countermeasures. Water Research 79, 128-146.

733 Dong, Y., Zhao, Y., Chen, Y., Feng, Y., Zhu, M., Ju, C., Zhang, B., Liu, H., Xu, J.,
734 2018. Graphdiyne-hybridized N-doped TiO_2 nanosheets for enhanced visible light

735 photocatalytic activity. Journal of Materials Science 53, 8921-8932.
736 Fang, Y., Xue, Y., Hui, L., Yu, H., Liu, Y., Xing, C., Lu, F., He, F., Liu, H., Li, Y., 2019.
737 In situ growth of graphdiyne based heterostructure: Toward efficient overall water
738 splitting. Nano Energy 59, 591-597.
739 Feng, S.H., Li, G.H., 2017. Chapter 4 - Hydrothermal and Solvothermal Syntheses. in:
740 Xu, R., Xu, Y. (Eds.). Modern Inorganic Synthetic Chemistry (Second Edition).
741 Elsevier, Amsterdam, pp. 73-104.
742 Fomina, L., Vazquez, B., Tkatchouk, E., Fomine, S., 2002. The Glaser reaction
743 mechanism. A DFT study. Tetrahedron 58, 6741-6747.
744 Góral, A., Lityńska-Dobrzyńska, L., Kot, M., 2017. Effect of Surface Roughness and
745 Structure Features on Tribological Properties of Electrodeposited Nanocrystalline
746 Ni and Ni/Al_2O_3 Coatings. Journal of Materials Engineering and Performance 26,
747 2118-2128.
748 Gao, G., O'Mullane, A.P., Du, A., 2017. 2D MXenes: A New Family of Promising
749 Catalysts for the Hydrogen Evolution Reaction. ACS Catalysis 7, 494-500.
750 Gao, X., Liu, H., Wang, D., Zhang, J., 2019. Graphdiyne: synthesis, properties, and
751 applications. Chemical Society Reviews 48, 908-936.
752 Geng, D., Yang, S., Zhang, Y., Yang, J., Liu, J., Li, R., Sham, T.K., Sun, X., Ye, S.,
753 Knights, S., 2011. Nitrogen doping effects on the structure of graphene. Applied
754 Surface Science 257, 9193-9198.
755 Haley, M.M., Brand, S.C., Pak, J.J., 1997. Carbon Networks Based on
756 Dehydrobenzoannulenes: Synthesis of Graphdiyne Substructures. Angewandte

Chemie International Edition in English 36, 836-838.

Han, Y.Y., Lu, X.L., Tang, S.F., Yin, X.P., Wei, Z.W., Lu, T.B., 2018. Metal-Free 2D/2D Heterojunction of Graphitic Carbon Nitride/Graphdiyne for Improving the Hole Mobility of Graphitic Carbon Nitride. Advanced Energy Materials 8, 1702992.

He, J., Li, X., Lu, T., Shen, X., Wang, N., Huang, C., 2019. Graphdiyne applied for electrochemical energy storage. Dalton Transactions 48, 14566-14574.

He, J., Ma, S.Y., Zhou, P., Zhang, C.X., He, C., Sun, L.Z., 2012. Magnetic Properties of Single Transition-Metal Atom Absorbed Graphdiyne and Graphyne Sheet from DFT+U Calculations. The Journal of Physical Chemistry C 116, 26313-26321.

Hisatomi, T., Domen, K., 2019. Reaction systems for solar hydrogen production via water splitting with particulate semiconductor photocatalysts. Nature Catalysis 2, 387-399.

Huang, C., Li, C., Shi, G., 2012. Graphene based catalysts. Energy & Environmental Science 5, 8848-8868.

Huang, C., Li, Y., Wang, N., Xue, Y., Zuo, Z., Liu, H., Li, Y., 2018. Progress in Research into 2D Graphdiyne-Based Materials. Chemical Reviews 118, 7744-7803.

Huang, C., Zhang, S., Liu, H., Li, Y., Cui, G., Li, Y., 2015. Graphdiyne for high capacity and long-life lithium storage. Nano Energy 11, 481-489.

Hui, L., Jia, D., Yu, H., Xue, Y., Li, Y., 2019a. Ultrathin Graphdiyne-Wrapped Iron Carbonate Hydroxide Nanosheets toward Efficient Water Splitting. ACS Applied

779 Materials & Interfaces 11, 2618-2625.
780 Hui, L., Xue, Y., He, F., Jia, D., Li, Y., 2019b. Efficient hydrogen generation on
781 graphdiyne-based heterostructure. Nano Energy 55, 135-142.
782 Hui, L., Xue, Y., Yu, H., Liu, Y., Fang, Y., Xing, C., Huang, B., Li, Y., 2019c. Highly
783 Efficient and Selective Generation of Ammonia and Hydrogen on a
784 Graphdiyne-Based Catalyst. Journal of the American Chemical Society 141,
785 10677-10683.
786 Iqbal, M.Z., Siddique, S., 2018. Recent progress in efficiency of hydrogen evolution
787 process based photoelectrochemical cell. International Journal of Hydrogen
788 Energy 43, 21502-21523.
789 Ivanovskaya, A., Singh, N., Liu, R.F., Kreutzer, H., Baltrusaitis, J., Van Nguyen, T.,
790 Metiu, H., McFarland, E., 2013. Transition Metal Sulfide Hydrogen Evolution
791 Catalysts for Hydrobromic Acid Electrolysis. Langmuir 29, 480-492.
792 Jin, J., Guo, M., Liu, J., Liu, J., Zhou, H., Li, J., Wang, L., Liu, H., Li, Y., Zhao, Y.,
793 Chen, C., 2018. Graphdiyne Nanosheet-Based Drug Delivery Platform for
794 Photothermal/Chemotherapy Combination Treatment of Cancer. ACS Applied
795 Materials & Interfaces 10, 8436-8442.
796 Kim, M., Park, J.N., Kim, H., Song, S., Lee, W.H., 2006. The preparation of Pt/C
797 catalysts using various carbon materials for the cathode of PEMFC. Journal of
798 Power Sources 163, 93-97.
799 Kuang, P., Zhu, B., Li, Y., Liu, H., Yu, J., Fan, K., 2018. Graphdiyne: a superior
800 carbon additive to boost the activity of water oxidation catalysts. Nanoscale

Horizons 3, 317-326.

Landrigan, P.J., Fuller, R., Fisher, S., Suk, W.A., Sly, P., Chiles, T.C., Bose-O'Reilly, S., 2019. Pollution and children's health. Science of The Total Environment 650, 2389-2394.

Lee, J., Kim, K.H., Kwon, E.E., 2017. Biochar as a Catalyst. Renewable and Sustainable Energy Reviews 77, 70-79.

Li, G., Li, Y., Liu, H., Guo, Y., Li, Y., Zhu, D., 2010. Architecture of graphdiyne nanoscale films. Chemical Communications 46, 3256-3258.

Li, J., Chen, Y., Gao, J., Zuo, Z., Li, Y., Liu, H., Li, Y., 2019a. Graphdiyne Sponge for Direct Collection of Oils from Water. ACS Applied Materials & Interfaces 11, 2591-2598.

Li, J., Zhong, L., Tong, L., Yu, Y., Liu, Q., Zhang, S., Yin, C., Qiao, L., Li, S., Si, R., Zhang, J., 2019b. Atomic Pd on Graphdiyne/Graphene Heterostructure as Efficient Catalyst for Aromatic Nitroreduction. Advanced Functional Materials, 1905423.

Li, Y., Xu, L., Liu, H., Li, Y., 2014. Graphdiyne and graphyne: from theoretical predictions to practical construction. Chemical Society Reviews 43, 2572-2586.

Liu, J., Chen, C., Zhao, Y., 2019a. Progress and Prospects of Graphdiyne-Based Materials in Biomedical Applications. Advanced Materials 31, 1804386.

Liu, J., Ma, Q., Huang, Z., Liu, G., Zhang, H., 2019b. Recent Progress in Graphene-Based Noble-Metal Nanocomposites for Electrocatalytic Applications. Advanced Materials 31, 1800696.

823 Liu, N., Lu, N., Su, Y., Wang, P., Quan, X., 2019c. Fabrication of g-C_3N_4/Ti_3C_2
824 composite and its visible-light photocatalytic capability for ciprofloxacin
825 degradation. Separation and Purification Technology 211, 782-789.
826 Liu, R., Gao, X., Zhou, J., Xu, H., Li, Z., Zhang, S., Xie, Z., Zhang, J., Liu, Z., 2017.
827 Chemical Vapor Deposition Growth of Linked Carbon Monolayers with
828 Acetylenic Scaffoldings on Silver Foil. Advanced Materials 29, 1604665.
829 Liu, R., Liu, H., Li, Y., Yi, Y., Shang, X., Zhang, S., Yu, X., Zhang, S., Cao, H., Zhang,
830 G., 2014. Nitrogen-doped graphdiyne as a metal-free catalyst for
831 high-performance oxygen reduction reactions. Nanoscale 6, 11336-11343.
832 Liu, X., Dai, L., 2016. Carbon-based metal-free catalysts. Nature Reviews Materials 1,
833 16064.
834 Long, M., Tang, L., Wang, D., Li, Y., Shuai, Z., 2011. Electronic Structure and Carrier
835 Mobility in Graphdiyne Sheet and Nanoribbons: Theoretical Predictions. ACS
836 Nano 5, 2593-2600.
837 Lu, Y., Song, S., Wang, R., Liu, Z., Meng, J., Sweetman, A.J., Jenkins, A., Ferrier,
838 R.C., Li, H., Luo, W., Wang, T., 2015. Impacts of soil and water pollution on food
839 safety and health risks in China. Environment International 77, 5-15.
840 Lu, Z., Li, S., Lv, P., He, C., Ma, D., Yang, Z., 2016. First principles study on the
841 interfacial properties of NM/graphdiyne (NM=Pd, Pt, Rh and Ir): The
842 implications for NM growing. Applied Surface Science 360, 1-7.
843 Lv, J., Wang, Z., Miura, H., 2018. Facile synthesis of mesoporous NiO nanoflakes on
844 graphene foam and its electrochemical properties for supercapacitor application.

845 Solid State Communications 269, 45-49.
846 Lv, J.X., Zhang, Z.M., Wang, J., Lu, X.L., Zhang, W., Lu, T.B., 2019. In Situ
847 Synthesis of CdS/Graphdiyne Heterojunction for Enhanced Photocatalytic
848 Activity of Hydrogen Production. ACS Applied Materials & Interfaces 11,
849 2655-2661.
850 Lv, Q., Si, W., Yang, Z., Wang, N., Tu, Z., Yi, Y., Huang, C., Jiang, L., Zhang, M., He,
851 J., Long, Y., 2017. Nitrogen-Doped Porous Graphdiyne: A Highly Efficient
852 Metal-Free Electrocatalyst for Oxygen Reduction Reaction. ACS Applied
853 Materials & Interfaces 9, 29744-29752.
854 Maggio, G., Nicita, A., Squadrito, G., 2019. How the hydrogen production from RES
855 could change energy and fuel markets: A review of recent literature. International
856 Journal of Hydrogen Energy 44, 11371-11384.
857 Mashhadzadeh, A.H., Vahedi, A.M., Ardjmand, M., Ahangari, M.G., 2016.
858 Investigation of heavy metal atoms adsorption onto graphene and graphdiyne
859 surface: A density functional theory study. Superlattices and Microstructures 100,
860 1094-1102.
861 Matsuoka, R., Sakamoto, R., Hoshiko, K., Sasaki, S., Masunaga, H., Nagashio, K.,
862 Nishihara, H., 2017. Crystalline Graphdiyne Nanosheets Produced at a
863 Gas/Liquid or Liquid/Liquid Interface. Journal of the American Chemical Society
864 139, 3145-3152.
865 Molnár, Á., Papp, A., 2017. Catalyst recycling—A survey of recent progress and
866 current status. Coordination Chemistry Reviews 349, 1-65.

867 Morales-Guio, C.G., Stern, L.A., Hu, X., 2014. Nanostructured hydrotreating catalysts
868 for electrochemical hydrogen evolution. Chemical Society Reviews 43,
869 6555-6569.
870 Musa, S.D., Zhonghua, T., Ibrahim, A.O., Habib, M., 2018. China's energy status: A
871 critical look at fossils and renewable options. Renewable and Sustainable Energy
872 Reviews 81, 2281-2290.
873 Naseri, A., Samadi, M., Pourjavadi, A., Moshfegh, A.Z., Ramakrishna, S., 2017.
874 Graphitic carbon nitride ($g\text{-}C_3N_4$)-based photocatalysts for solar hydrogen
875 generation: recent advances and future development directions. Journal of
876 Materials Chemistry A 5, 23406-23433.
877 Nehring, R., 2009. Traversing the mountaintop: world fossil fuel production to 2050.
878 Philosophical Transactions of the Royal Society B: Biological Sciences 364,
879 3067-3079.
880 Parmon, V.N., Simagina, V.I., Milova, L.P., 2010. Precious metals in catalyst
881 production. Catalysis in Industry 2, 199-205.
882 Poudyal, R., Loskot, P., Nepal, R., Parajuli, R., Khadka, S.K., 2019. Mitigating the
883 current energy crisis in Nepal with renewable energy sources. Renewable and
884 Sustainable Energy Reviews 116, 109388.
885 Qi, J., Zhang, W., Cao, R., 2018. Solar-to-Hydrogen Energy Conversion Based on
886 Water Splitting. Advanced Energy Materials 8, 1701620.
887 Qiao, F., Liang, Q., Yang, J., Chen, Z., Xu, Q., 2019. A Facile Approach of
888 Fabricating Various ZnO Microstructures via Electrochemical Deposition. Journal

889 of Electronic Materials 48, 2338-2342.
890 Saha, N., Rahman, M.S., Ahmed, M.B., Zhou, J.L., Ngo, H.H., Guo, W., 2017.
891 Industrial metal pollution in water and probabilistic assessment of human health
892 risk. Journal of Environmental Management 185, 70-78.
893 Salgot, M., Folch, M., 2018. Wastewater treatment and water reuse. Current Opinion
894 in Environmental Science & Health 2, 64-74.
895 Saraswat, S.K., Rodene, D.D., Gupta, R.B., 2018. Recent advancements in
896 semiconductor materials for photoelectrochemical water splitting for hydrogen
897 production using visible light. Renewable and Sustainable Energy Reviews 89,
898 228-248.
899 Shafiee, S., Topal, E., 2009. When will fossil fuel reserves be diminished? Energy
900 Policy 37, 181-189.
901 Shang, H., Zuo, Z., Zheng, H., Li, K., Tu, Z., Yi, Y., Liu, H., Li, Y., Li, Y., 2018.
902 N-doped graphdiyne for high-performance electrochemical electrodes. Nano
903 Energy 44, 144-154.
904 Shen, H., Li, Y., Shi, Z., 2019. A Novel Graphdiyne-Based Catalyst for Effective
905 Hydrogenation Reaction. ACS Applied Materials & Interfaces 11, 2563-2570.
906 Shen, H., Zhou, W., He, F., Gu, Y., Li, Y., Li, Y., 2020. A
907 dehydrobenzoannulene-based three dimensional graphdiyne for photocatalytic
908 hydrogen generation using Pt nanoparticles as a co-catalyst and triethanolamine
909 as a sacrificial electron donor. Journal of Materials Chemistry A 8, 4850-4855.
910 Sheng, W., Myint, M., Chen, J.G., Yan, Y., 2013. Correlating the hydrogen evolution

911 reaction activity in alkaline electrolytes with the hydrogen binding energy on
912 monometallic surfaces. Energy & Environmental Science 6, 1509-1512.
913 Shi, G., Yu, C., Fan, Z., Li, J., Yuan, M., 2019. Graphdiyne-Supported NiFe Layered
914 Double Hydroxide Nanosheets as Functional Electrocatalysts for Oxygen
915 Evolution. ACS Applied Materials & Interfaces 11, 2662-2669.
916 Shinagawa, T., Garcia-Esparza, A.T., Takanabe, K., 2015. Insight on Tafel slopes from
917 a microkinetic analysis of aqueous electrocatalysis for energy conversion.
918 Scientific Reports 5, 13801.
919 Si, H.Y., Deng, Q.X., Chen, L.C., Wang, L., Liu, X.Y., Wu, W.S., Zhang, Y.H., Zhou,
920 J.M., Zhang, H.L., 2019. Hierarchical Graphdiyne@NiFe layered double
921 hydroxide heterostructures as a bifunctional electrocatalyst for overall water
922 splitting. Journal of Alloys and Compounds 794, 261-267.
923 Smestad, G.P., Steinfeld, A., 2012. Review: Photochemical and Thermochemical
924 Production of Solar Fuels from H2O and CO2 Using Metal Oxide Catalysts.
925 Industrial & Engineering Chemistry Research 51, 11828-11840.
926 Song, B., Xu, P., Zeng, G., Gong, J., Zhang, P., Feng, H., Liu, Y., Ren, X., 2018.
927 Carbon nanotube-based environmental technologies: the adopted properties,
928 primary mechanisms, and challenges. Reviews in Environmental Science and
929 Bio/Technology 17, 571-590.
930 Song, B., Zeng, Z., Zeng, G., Gong, J., Xiao, R., Ye, S., Chen, M., Lai, C., Xu, P.,
931 Tang, X., 2019. Powerful combination of g-C_3N_4 and LDHs for enhanced
932 photocatalytic performance: A review of strategy, synthesis, and applications.

933 Advances in Colloid and Interface Science 272, 101999.
934 Stern, A.G., 2018. A new sustainable hydrogen clean energy paradigm. International
935 Journal of Hydrogen Energy 43, 4244-4255.
936 Sun, M., Wu, T., Xue, Y., Dougherty, A.W., Huang, B., Li, Y., Yan, C.H., 2019.
937 Mapping of atomic catalyst on graphdiyne. Nano Energy 62, 754-763.
938 Teixeira, S., Gurke, R., Eckert, H., Kühn, K., Fauler, J., Cuniberti, G., 2016.
939 Photocatalytic degradation of pharmaceuticals present in conventional treated
940 wastewater by nanoparticle suspensions. Journal of Environmental Chemical
941 Engineering 4, 287-292.
942 Thangavel, S., Krishnamoorthy, K., Krishnaswamy, V., Raju, N., Kim, S.J., Venugopal,
943 G., 2015. Graphdiyne–ZnO Nanohybrids as an Advanced Photocatalytic Material.
944 The Journal of Physical Chemistry C 119, 22057-22065.
945 Wang, S., Yi, L., Halpert, J.E., Lai, X., Liu, Y., Cao, H., Yu, R., Wang, D., Li, Y., 2012.
946 A Novel and Highly Efficient Photocatalyst Based on P25–Graphdiyne
947 Nanocomposite. Small 8, 265-271.
948 Wang, W., Zeng, Z., Zeng, G., Zhang, C., Xiao, R., Zhou, C., Xiong, W., Yang, Y., Lei,
949 L., Liu, Y., Huang, D., Cheng, M., Yang, Y., Fu, Y., Luo, H., Zhou, Y., 2019.
950 Sulfur doped carbon quantum dots loaded hollow tubular g-C_3N_4 as novel
951 photocatalyst for destruction of *Escherichia coli* and tetracycline degradation
952 under visible light. Chemical Engineering Journal 378, 122132.
953 Wang, X.X., Tan, Z.H., Zeng, M., Wang, J.N., 2014. Carbon nanocages: A new
954 support material for Pt catalyst with remarkably high durability. Scientific

955 Reports 4, 4437.
956 Wu, P., Du, P., Zhang, H., Cai, C., 2014. Graphdiyne as a metal-free catalyst for
957 low-temperature CO oxidation. Physical Chemistry Chemical Physics 16,
958 5640-5648.
959 Wu, Z., Yuan, X., Wang, H., Wu, Z., Jiang, L., Wang, H., Zhang, L., Xiao, Z., Chen,
960 X., Zeng, G., 2017. Facile synthesis of a novel full-spectrum-responsive
961 Co2.67S4 nanoparticles for UV-, vis- and NIR-driven photocatalysis. Applied
962 Catalysis B: Environmental 202, 104-111.
963 Xiong, W., Zeng, G., Yang, Z., Zhou, Y., Zhang, C., Cheng, M., Liu, Y., Hu, L., Wan,
964 J., Zhou, C., Xu, R., Li, X., 2018. Adsorption of tetracycline antibiotics from
965 aqueous solutions on nanocomposite multi-walled carbon nanotube
966 functionalized MIL-53(Fe) as new adsorbent. Science of The Total Environment
967 627, 235-244.
968 Xu, B., Ahmed, M.B., Zhou, J.L., Altaee, A., Wu, M., Xu, G., 2017. Photocatalytic
969 removal of perfluoroalkyl substances from water and wastewater: Mechanism,
970 kinetics and controlling factors. Chemosphere 189, 717-729.
971 Xu, Q., Zhu, B., Cheng, B., Yu, J., Zhou, M., Ho, W., 2019. Photocatalytic H_2
972 evolution on graphdiyne/g-C_3N_4 hybrid nanocomposites. Applied Catalysis B:
973 Environmental 255, 117770.
974 Xue, Y., Huang, B., Yi, Y., Guo, Y., Zuo, Z., Li, Y., Jia, Z., Liu, H., Li, Y., 2018.
975 Anchoring zero valence single atoms of nickel and iron on graphdiyne for
976 hydrogen evolution. Nature Communications 9, 1460.

977 Xue, Y., Li, J., Xue, Z., Li, Y., Liu, H., Li, D., Yang, W., Li, Y., 2016. Extraordinarily
978 Durable Graphdiyne-Supported Electrocatalyst with High Activity for Hydrogen
979 Production at All Values of pH. ACS Applied Materials & Interfaces 8,
980 31083-31091.
981 Xue, Y., Zuo, Z., Li, Y., Liu, H., Li, Y., 2017. Graphdiyne-Supported $NiCo_2S_4$
982 Nanowires: A Highly Active and Stable 3D Bifunctional Electrode Material.
983 Small 13, 1700936.
984 Yan, Y., Miao, J., Yang, Z., Xiao, F.X., Yang, H.B., Liu, B., Yang, Y., 2015. Carbon
985 nanotube catalysts: recent advances in synthesis, characterization and
986 applications. Chemical Society Reviews 44, 3295-3346.
987 Yang, N., Liu, Y., Wen, H., Tang, Z., Zhao, H., Li, Y., Wang, D., 2013. Photocatalytic
988 Properties of Graphdiyne and Graphene Modified TiO_2: From Theory to
989 Experiment. ACS Nano 7, 1504-1512.
990 Yang, Y., Zeng, Z., Zeng, G., Huang, D., Xiao, R., Zhang, C., Zhou, C., Xiong, W.,
991 Wang, W., Cheng, M., Xue, W., Guo, H., Tang, X., He, D., 2019a. Ti_3C_2
992 Mxene/porous g-C_3N_4 interfacial Schottky junction for boosting spatial charge
993 separation in photocatalytic H_2O_2 production. Applied Catalysis B:
994 Environmental 258, 117956.
995 Yang, Y., Zhang, C., Huang, D., Zeng, G., Huang, J., Lai, C., Zhou, C., Wang, W., Guo,
996 H., Xue, W., Deng, R., Cheng, M., Xiong, W., 2019b. Boron nitride quantum dots
997 decorated ultrathin porous g-C_3N_4: Intensified exciton dissociation and charge
998 transfer for promoting visible-light-driven molecular oxygen activation. Applied

Catalysis B: Environmental 245, 87-99.

Yao, Y., Jin, Z., Chen, Y., Gao, Z., Yan, J., Liu, H., Wang, J., Li, Y., Liu, S., 2018. Graphdiyne-WS_2 2D-Nanohybrid electrocatalysts for high-performance hydrogen evolution reaction. Carbon 129, 228-235.

Yarger, M.S., Steinmiller, E.M.P., Choi, K.S., 2008. Electrochemical Synthesis of Zn−Al Layered Double Hydroxide (LDH) Films. Inorganic Chemistry 47, 5859-5865.

Yaseen, D.A., Scholz, M., 2019. Textile dye wastewater characteristics and constituents of synthetic effluents: a critical review. International Journal of Environmental Science and Technology 16, 1193-1226.

Ye, S., Yan, M., Tan, X., Liang, J., Zeng, G., Wu, H., Song, B., Zhou, C., Yang, Y., Wang, H., 2019. Facile assembled biochar-based nanocomposite with improved graphitization for efficient photocatalytic activity driven by visible light. Applied Catalysis B: Environmental 250, 78-88.

Yu, H., Xue, Y., Huang, B., Hui, L., Zhang, C., Fang, Y., Liu, Y., Zhao, Y., Li, Y., Liu, H., Li, Y., 2019. Ultrathin Nanosheet of Graphdiyne-Supported Palladium Atom Catalyst for Efficient Hydrogen Production. iScience 11, 31-41.

Yu, H., Xue, Y., Hui, L., Zhang, C., Zhao, Y., Li, Z., Li, Y., 2018. Controlled Growth of MoS2 Nanosheets on 2D N-Doped Graphdiyne Nanolayers for Highly Associated Effects on Water Reduction. Advanced Functional Materials 28, 1707564.

Zhai, Y., Zhu, Z., Dong, S., 2015. Carbon-Based Nanostructures for Advanced

Catalysis. ChemCatChem 7, 2806-2815.

Zhang, H., Zhao, X., Zhang, M., Luo, Y., Li, G., Zhao, M., 2013. Three-dimensional diffusion of molecular hydrogen in graphdiyne: a first-principles study. Journal of Physics D: Applied Physics 46, 495307.

Zhang, L., Doyle-Davis, K., Sun, X., 2019. Pt-Based electrocatalysts with high atom utilization efficiency: from nanostructures to single atoms. Energy & Environmental Science 12, 492-517.

Zhang, P., Lou, X.W., 2019. Design of Heterostructured Hollow Photocatalysts for Solar-to-Chemical Energy Conversion. Advanced Materials 31, 1900281.

Zhang, X., Zhu, M., Chen, P., Li, Y., Liu, H., Li, Y., Liu, M., 2015. Pristine graphdiyne-hybridized photocatalysts using graphene oxide as a dual-functional coupling reagent. Physical Chemistry Chemical Physics 17, 1217-1225.

Zhao, J., Chen, Z., Zhao, J., 2019. Metal-free graphdiyne doped with sp-hybridized boron and nitrogen atoms at acetylenic sites for high-efficiency electroreduction of CO2 to CH4 and C2H4. Journal of Materials Chemistry A 7, 4026-4035.

Zhao, X., Tang, J., Yu, F., Ye, N., 2018a. Preparation of graphene nanoplatelets reinforcing copper matrix composites by electrochemical deposition. Journal of Alloys and Compounds 766, 266-273.

Zhao, Y., Wan, J., Yao, H., Zhang, L., Lin, K., Wang, L., Yang, N., Liu, D., Song, L., Zhu, J., Gu, L., Liu, L., Zhao, H., Li, Y., Wang, D., 2018b. Few-layer graphdiyne doped with sp-hybridized nitrogen atoms at acetylenic sites for oxygen reduction electrocatalysis. Nature Chemistry 10, 924-931.

Zhou, C., Zeng, G., Huang, D., Luo, Y., Cheng, M., Liu, Y., Xiong, W., Yang, Y., Song, B., Wang, W., Shao, B., Li, Z., 2020. Distorted polymeric carbon nitride via carriers transfer bridges with superior photocatalytic activity for organic pollutants oxidation and hydrogen production under visible light. Journal of Hazardous Materials 386, 121947.

Zhou, W., Jia, J., Lu, J., Yang, L., Hou, D., Li, G., Chen, S., 2016. Recent developments of carbon-based electrocatalysts for hydrogen evolution reaction. Nano Energy 28, 29-43.

Zhou, W., Shen, H., Wu, C., Tu, Z., He, F., Gu, Y., Xue, Y., Zhao, Y., Yi, Y., Li, Y., Li, Y., 2019. Direct synthesis of crystalline graphdiyne analogue based on supramolecular interactions. Journal of the American Chemical Society 141, 48-52.

Zuo, Z., Shang, H., Chen, Y., Li, J., Liu, H., Li, Y., Li, Y., 2017. A facile approach for graphdiyne preparation under atmosphere for an advanced battery anode. Chemical Communications 53, 8074-8077.

Zuo, Z., Wang, D., Zhang, J., Lu, F., Li, Y., 2019. Synthesis and Applications of Graphdiyne-Based Metal-Free Catalysts. Advanced Materials 31, 1803762.

Figure 1

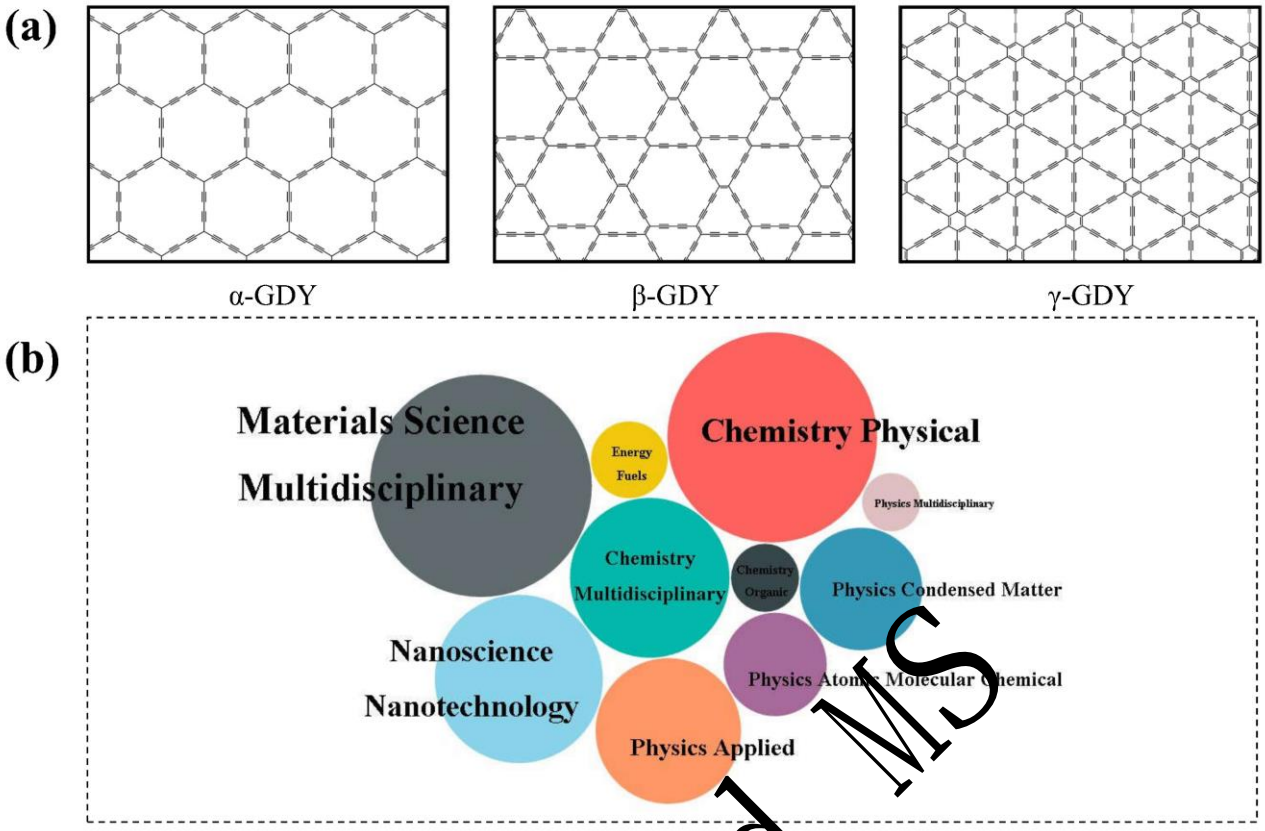

Fig. 1. Schematic diagram of different GDY structures (a), and TOP 10 Web of Science Categories for GDY publications (b). The category analysis was based on the data extracted from Web of Science Core Collection in December 2019 by searching publications containing "graphdiyne" in the topic. A larger circle size indicates a higher proportion of publications belonging to the corresponding category in the total.

Figure 2

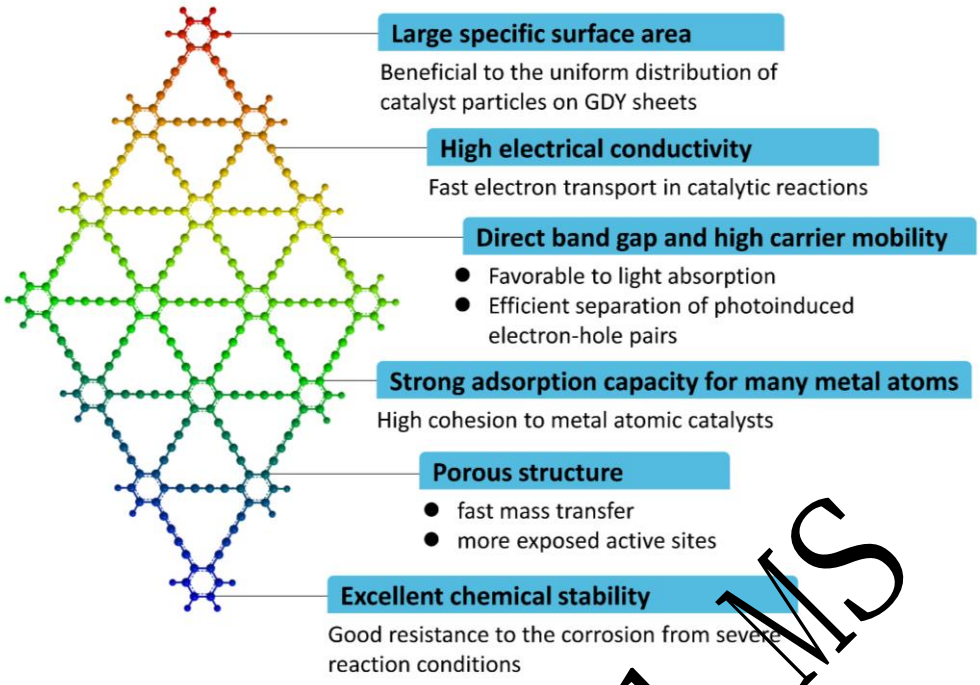

Fig. 2. Main properties and advantages of GDY for its application as a catalyst support.

Figure 3

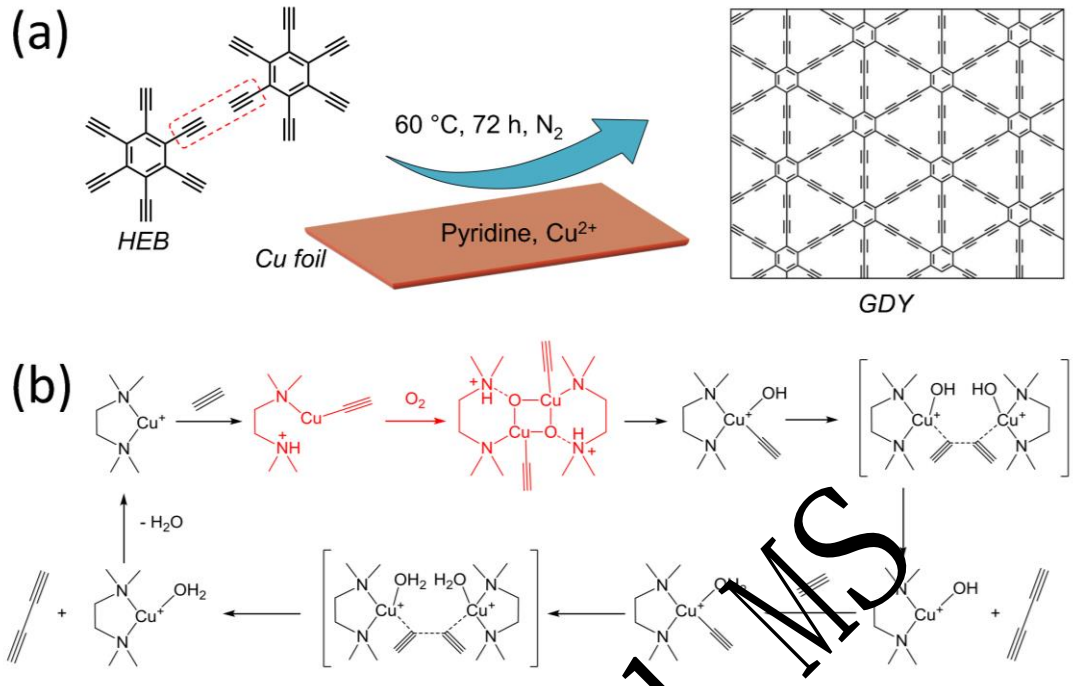

Fig. 3. Schematic diagram of synthesizing GDY via an in-situ cross-coupling reaction of HEB monomers on a Cu foil (a), and potential mechanism of Glaser-Hay coupling reaction (b). The schematic diagram was drawn according to the method used by Li et al. (2010), and the reaction mechanism was illustrated according to the description by Fomina et al. (2002).

Figure 4

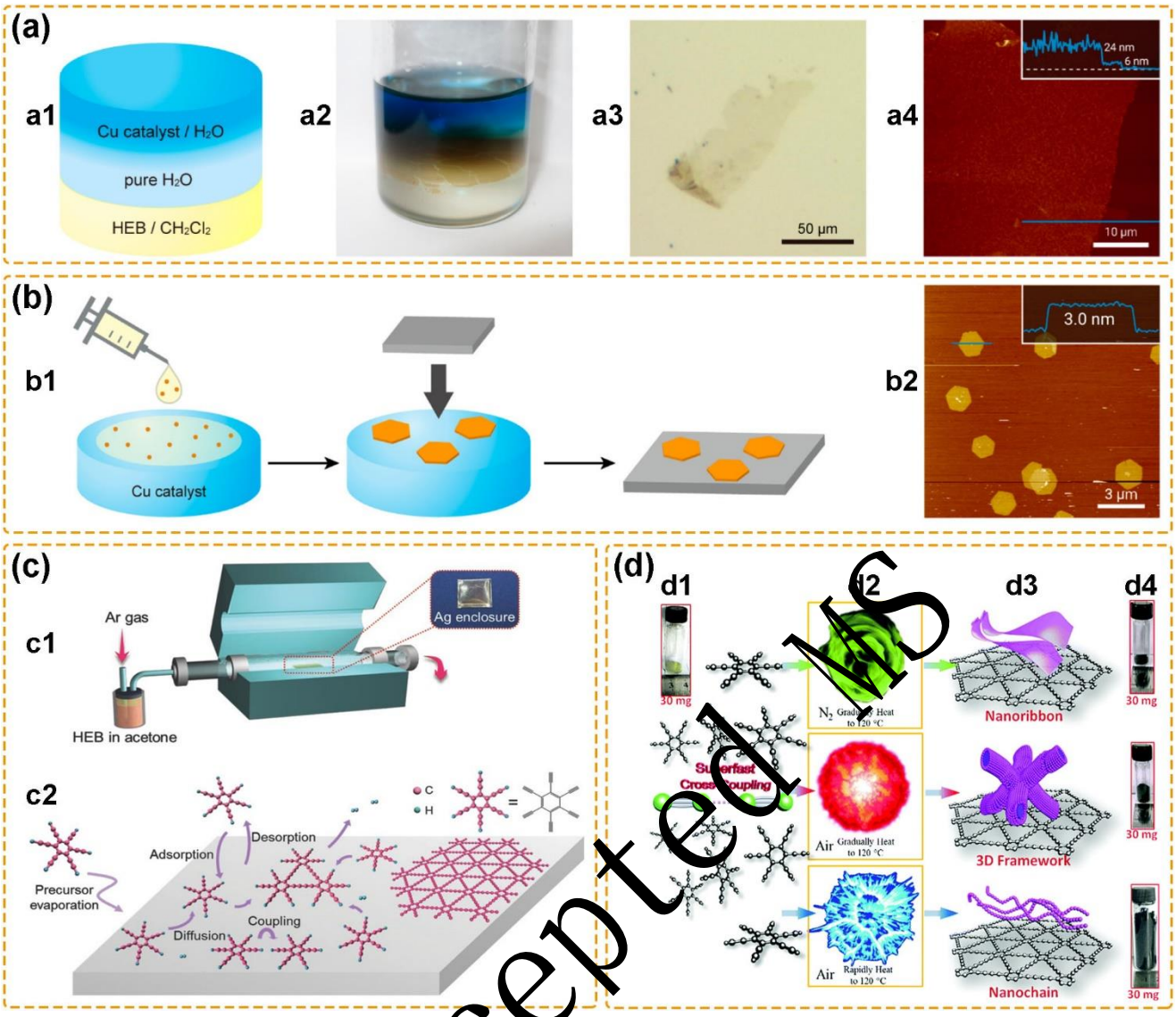

Fig. 4. Preparing GDY by liquid/liquid interfacial synthesis (a), gas/liquid interfacial synthesis (b), CVD method (c), and explosion method (d). Schematic diagram (a1) and a real photo (a2) of the GDY synthesis at liquid/liquid interface; optical microscope image (a3) and atomic force microscope image (a4) of the synthesized GDY sheet. Schematic diagram of the GDY synthesis at gas/liquid interface (b1) and atomic force microscope image of the synthesized GDY sheet (b2). Reproduced with permission from Matsuoka et al. (2017). Copyright 2017 American Chemical Society. Schematic diagram of the CVD system for synthesizing monolayer GDY sheet on Ag foil (c1) and the potential growth process of GDY (c2). Reproduced with permission from Liu et al. (2017). Copyright 2017 Wiley-VCH. A real photo of the precursor HEB in light yellow (d1), different thermal treatments for HEB coupling (d2), different morphology of the GDY products (d3), and real product photos showing the volume change (d4). Reproduced with permission from Zuo et al. (2017). Copyright 2017 The Royal Society of Chemistry.

Figure 5

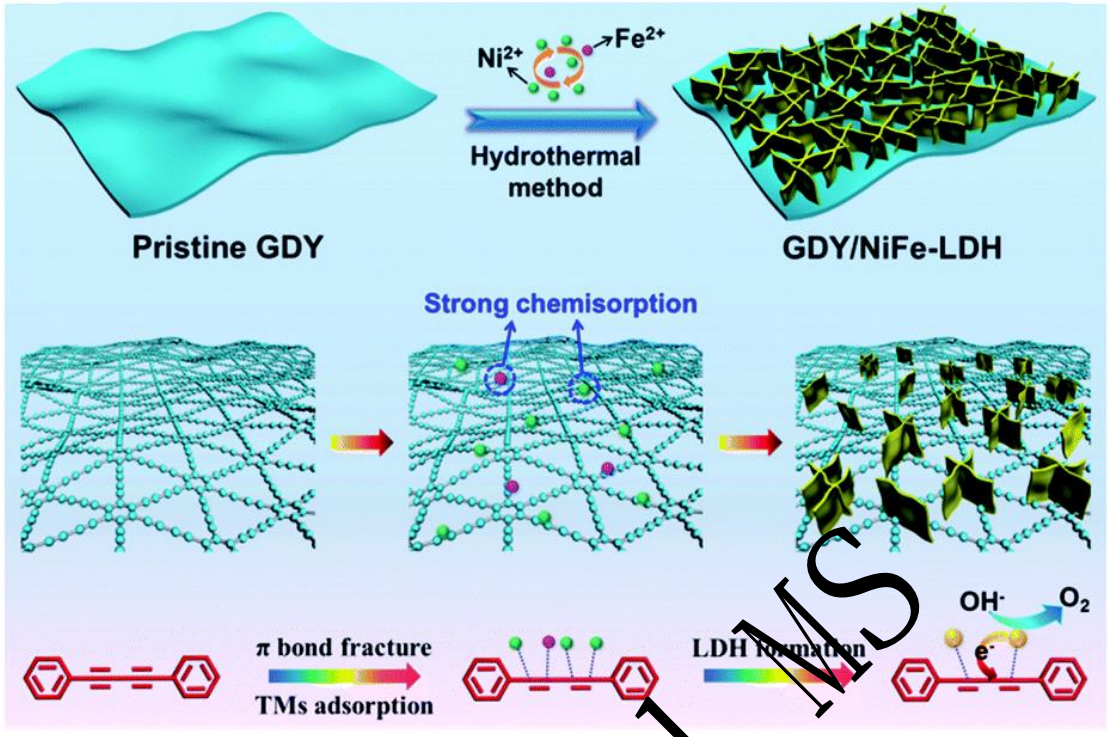

Fig. 5. Schematic diagram of synthesizing NiFe-LDH/GDY electrocatalyst by hydrothermal method. TMs: transition metals (referring to Ni and Fe ions here). Reproduced with permission from Kuang et al. (2018). Copyright 2018 The Royal Society of Chemistry.

Figure 6

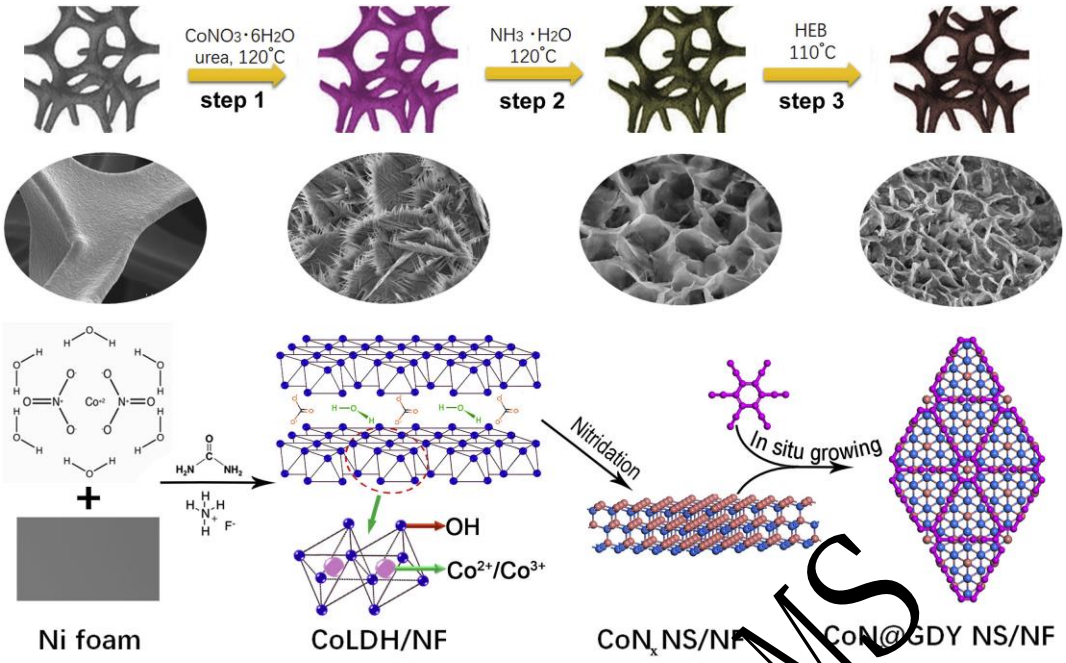

Fig. 6. Schematic diagram of synthesizing CoNx/GDY electrocatalyst by GDY in-situ growth. NS: nanosheet; NF: Ni foam. Reproduced with permission from Fang et al. (2019). Copyright 2019 Elsevier.

Figure 7

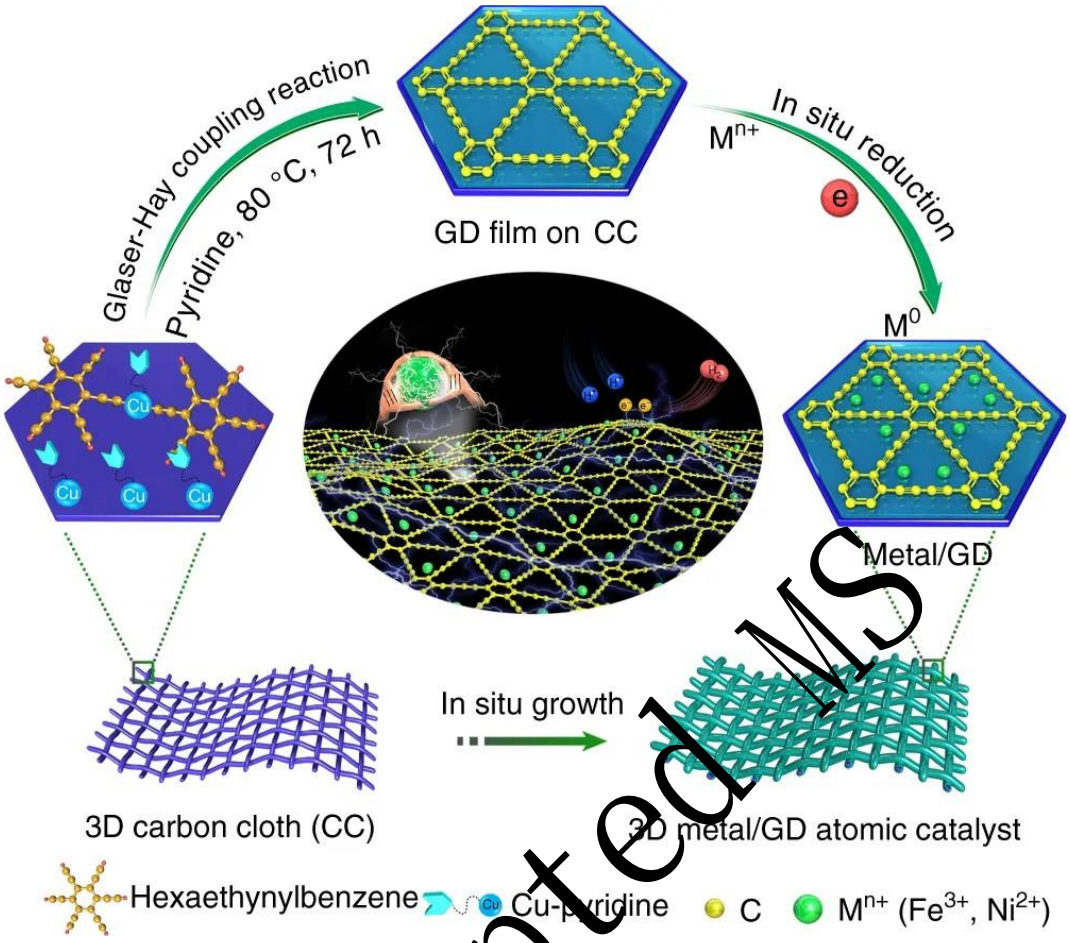

Fig. 7. Schematic diagram of synthesizing Ni0/GDY and Fe0/GDY catalysts by electrochemical deposition. Reproduced with permission from Xue et al. (2018). Copyright 2018 Springer Nature.

Figure 8

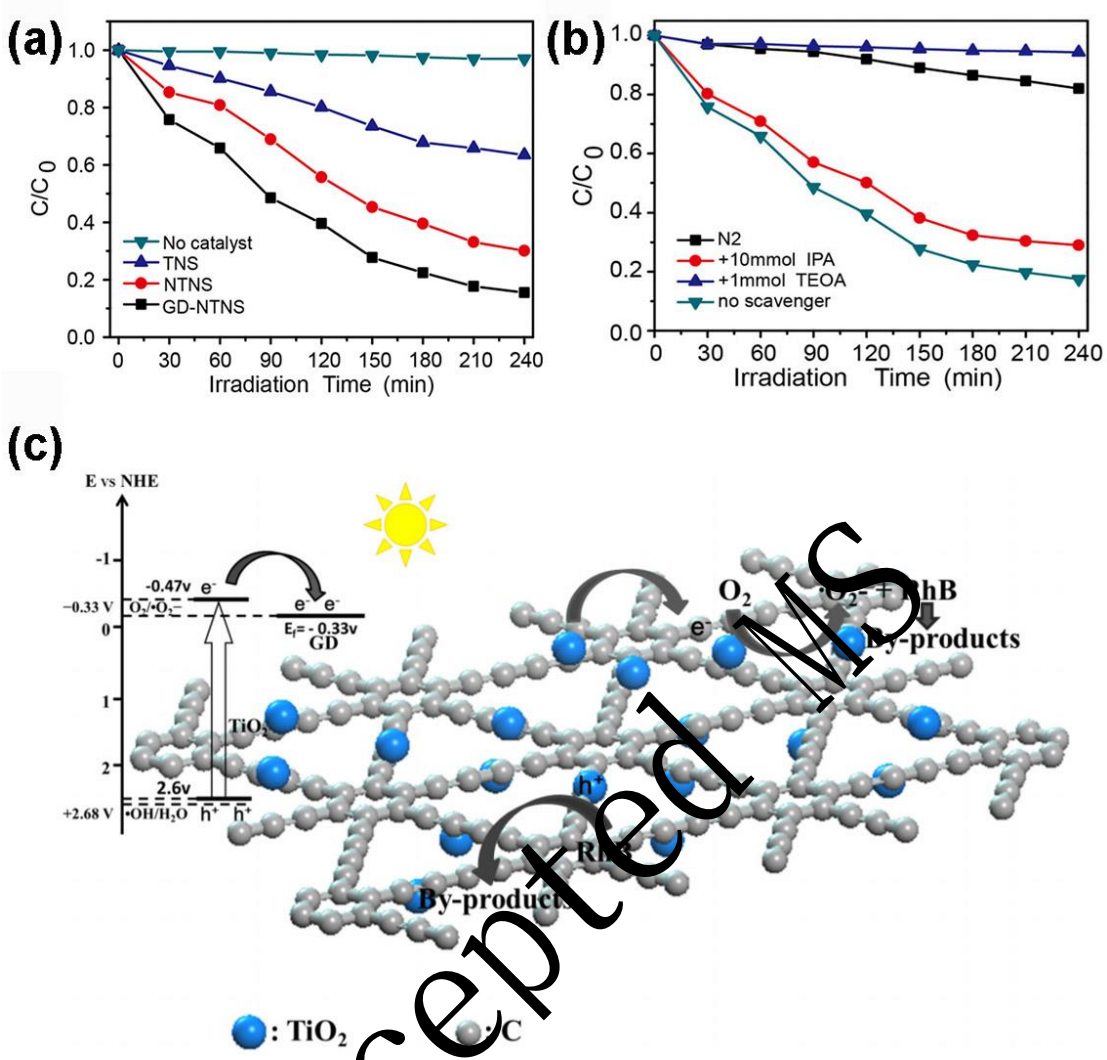

Fig. 8. Photocatalytic degradation of RhB with bare TiO2 nanosheets (TNS), N-doped TiO2 nanosheets (NTNS), and N-doped TiO2/GDY (GD-NTNS) under visible light irradiation (a), photocatalytic degradation of RhB with N-doped TiO2/GDY in the presence of different scavengers (b), and schematic diagram for possible mechanism of the photocatalytic degradation of RhB with N-doped TiO2/GDY under visible light irradiation (c). Reproduced with permission from Dong et al. (2018). Copyright 2018 Springer Nature.

Figure 9

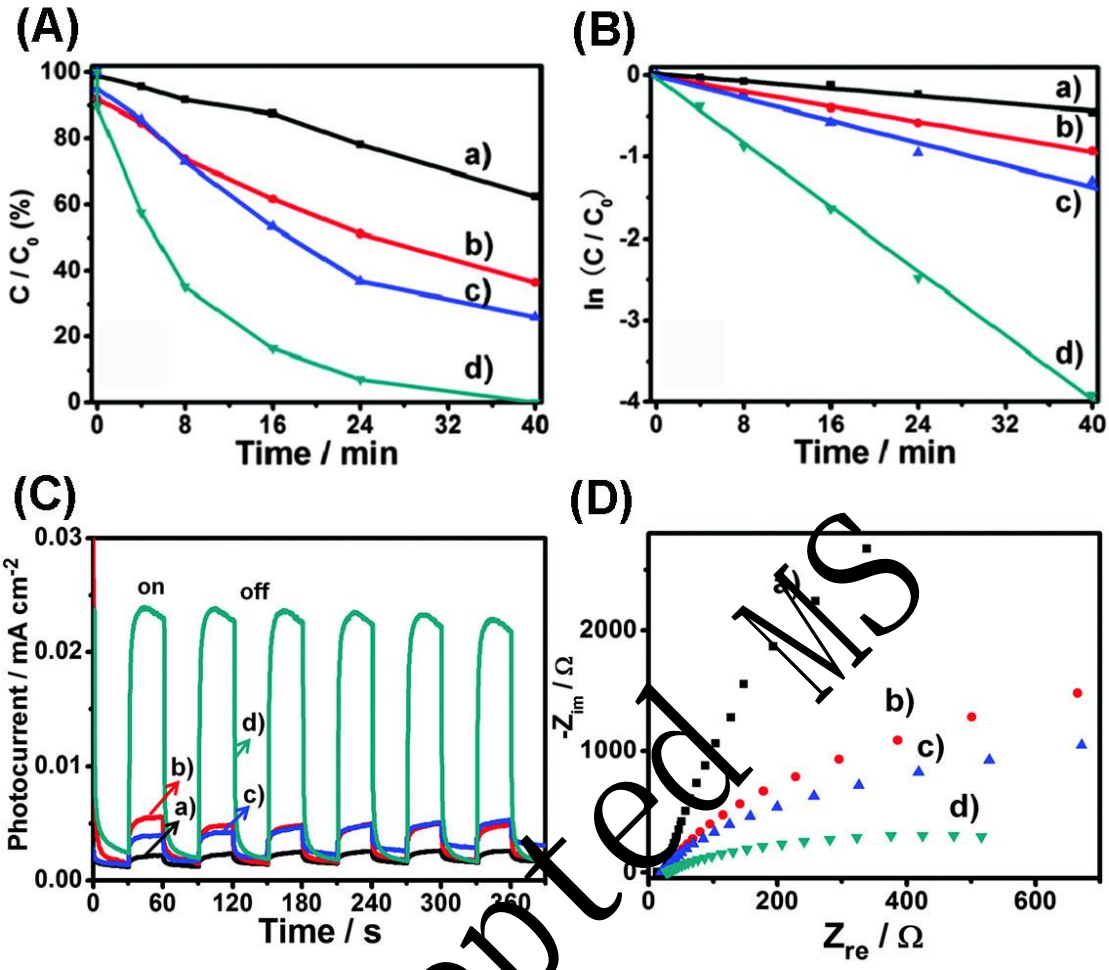

Fig. 9. Photocatalytic degradation of MO with different catalysts under visible light irradiation (A), kinetic linear simulation curves for the photocatalytic degradation performances (B), transient photocurrent responses (C) and electrochemical impedance spectra (D) of the indium tin oxide electrodes modified by different catalysts. The tested catalysts: Ag/AgBr (a), Ag/AgBr/GO (b), Ag/AgBr/GDY (c), and Ag/AgBr/GO/GDY (d). Reproduced with permission from Zhang et al. (2015). Copyright 2015 The PCCP Owner Societies.

Figure 10

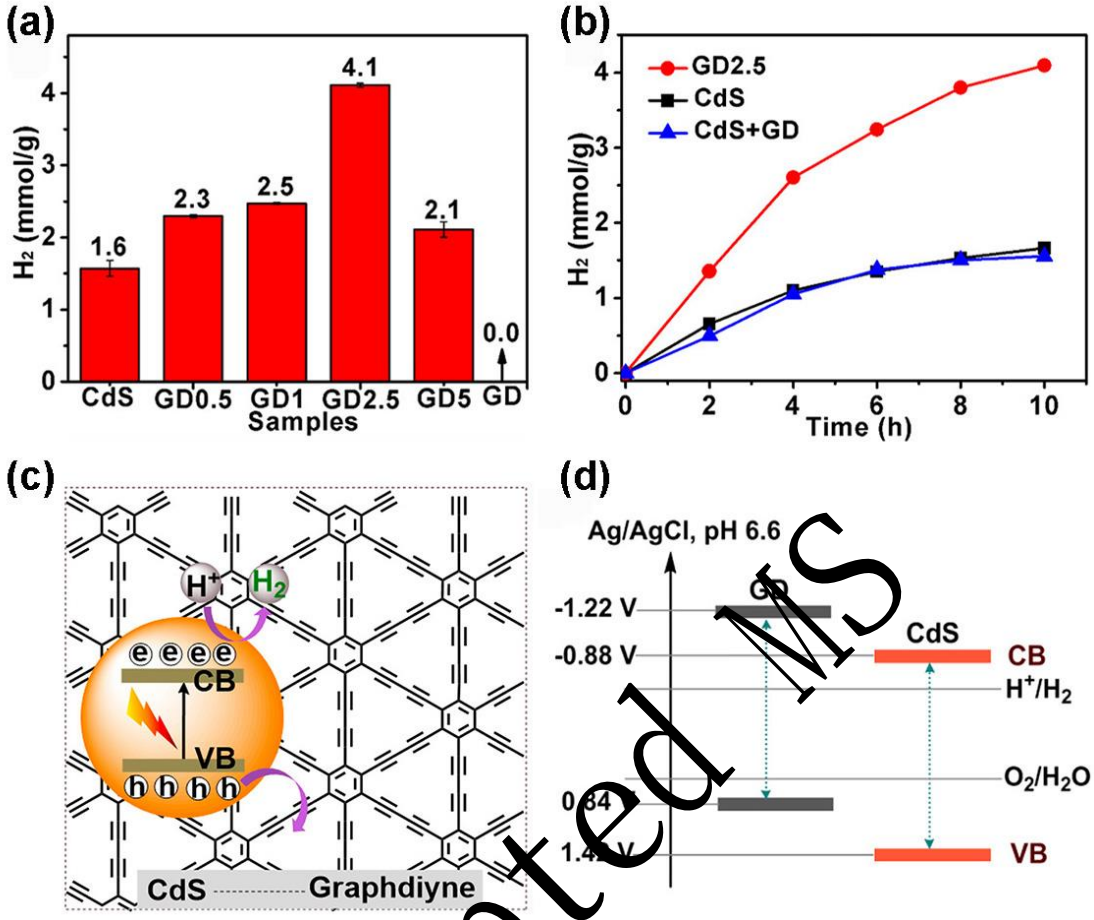

Fig. 10. The amount of hydrogen production with CdS, GDY (GD), and different CdS/GDY composites (GDn) in the photocatalytic water splitting (a), hydrogen evolution over time with GD2.5, CdS, and a physical mixture of GDY (2.5%, w/w) and CdS in the photocatalytic water splitting (b), schematic diagram for the possible mechanism of hydrogen production with CdS/GDY photocatalyst (c), and band structures of GDY and CdS (d). GDn: CdS/GDY composite synthesized by using n wt% GDY. Reproduced with permission from Lv et al. (2019). Copyright 2019 American Chemical Society.

Figure 11

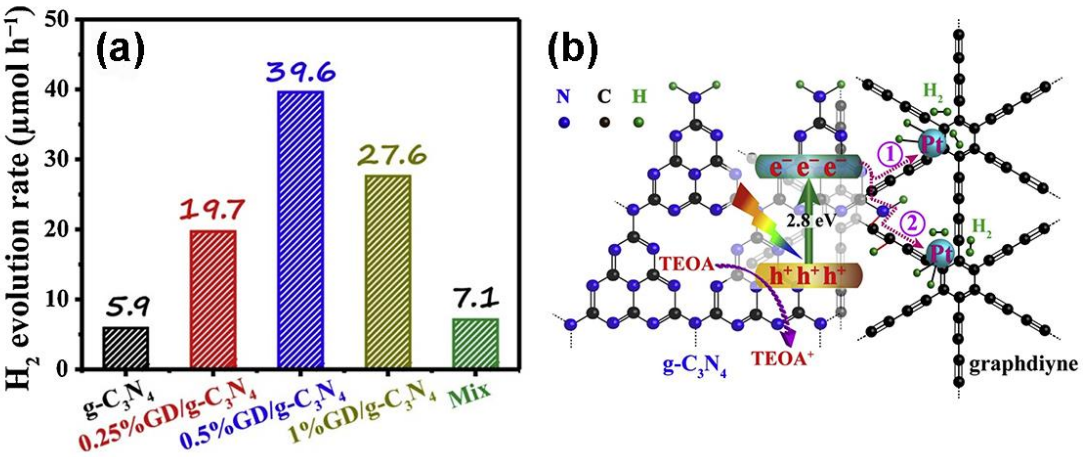

Fig. 11. Hydrogen evolution rates with different photocatalysts under visible light irradiation (a), and schematic diagram for the possible mechanism of hydrogen production with g-C3N4/GDY photocatalyst loaded with Pt NPs (b). Reproduced with permission from Xu et al. (2019). Copyright 2019 Elsevier.

Figure 12

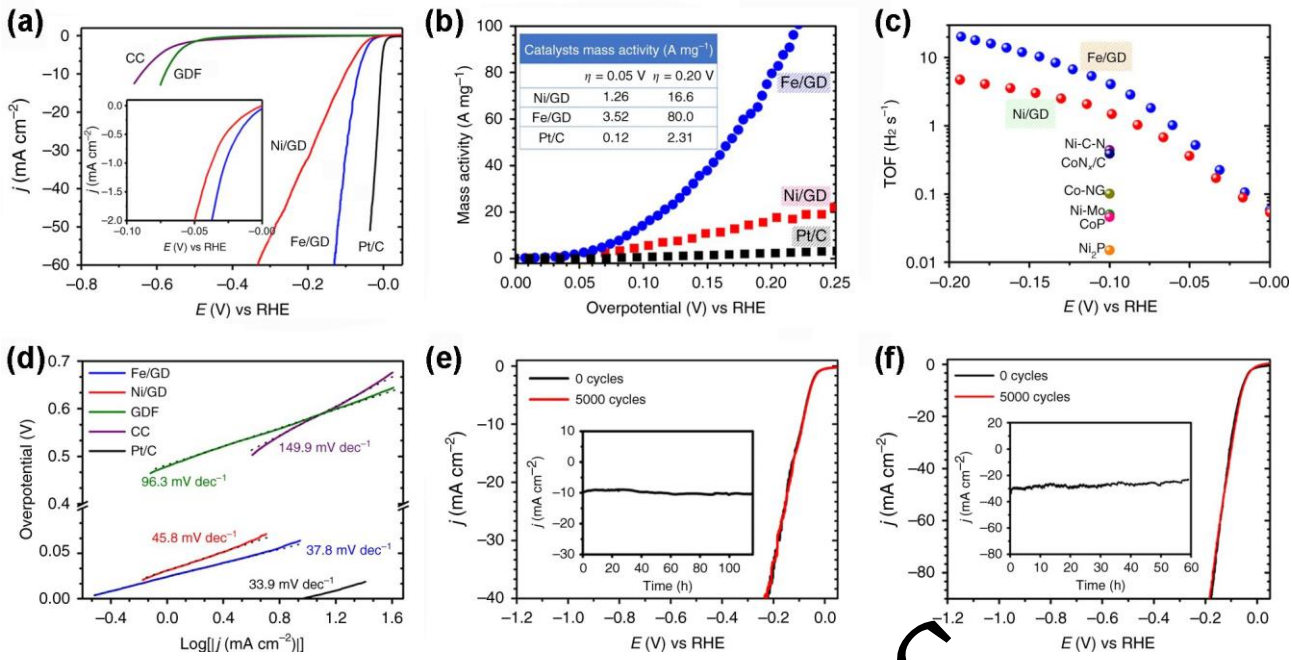

Fig. 12. HER polarization curves with a inset of the enlarged view for Ni0/GDY, Fe0/GDY near the onset region (a), mass activity of Ni0/GDY, Fe0/GDY, and Pt/C (b), TOF values of Ni0/GDY, Fe0/GDY, and some state-of-the-art HER electrocatalysts (c), Tafel plots of the studied electrocatalysts (d), and stability tests of Ni0/GDY (e), Fe0/GDY (f) with insets of the time-dependent current density curves. Fe/GD: Fe0/GDY, Ni/GD: Ni0/GDY, GDF: graphdiyne foam, CC, carbon cloth. Adapted with permission from Xue et al. (2018). Copyright 2018 Springer Nature.

Figure 13

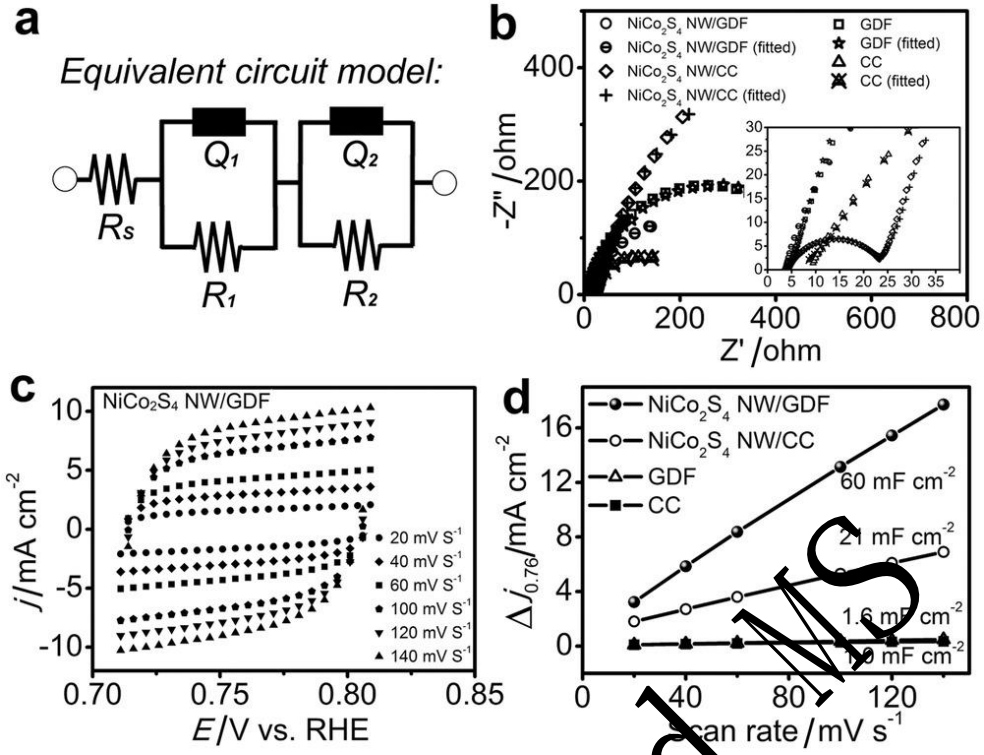

Fig. 13. The equivalent circuit model for EIS analysis of NiCo2S4 nanowires/GDY (a), Nyquist plots of the studied electrocatalysts in 1.0 M KOH electrolyte (b), CV curves of the NiCo2S4 nanowires/GDY in the potential range of 0.71–0.81 V versus RHE at different scan rates (c), and the capacitive currents at 0.76 V versus RHE as a function of scan rates for the studied electrocatalysts (d). CC: carbon cloth, GDF: graphdiyne foam, NiCo2S4 NW: NiCo2S4 nanowires. Rs: solution resistance, R1: charge transfer resistance, R2: hydrogen adsorption resistance, Q1 and Q2: constant phase elements. Reproduced with permission from Xue et al. (2017). Copyright 2017 Wiley-VCH.

Table 1 Some experiments for loading catalysts on GDY support.

Catalyst	Loading method	Reactants	Reaction conditions	Reference
TiO_2/GDY	Hydrothermal method	GDY, TiO_2 NPs	120 ℃, 3 h	Wang et al. (2012)
TiO_2/GDY	Hydrothermal method	GDY, TiO_2 NPs	120 ℃, 3 h	Yang et al. (2013)
ZnO/GDY	Hydrothermal method	GDY, $Zn(OAc)_2$, NaOH	180 ℃, 24 h	Thangavel et al. (2015)
N-doped TiO_2/GDY	Hydrothermal method	GDY, N-doped TiO_2 NPs	120 ℃, 3 h	Dong et al. (2018)
$NiCo_2S_4$ nanowires/GDY	Hydrothermal method	1) GDY, $Ni(NO_3)_2$, $Co(NO_3)_2$, urea 2) Ni-Co-precursor/GDY, Na_2S	1) 120 ℃, 8 h 2) 160 ℃, 8 h	Xue et al. (2017)
Ni-Fe-LDH/GDY	Hydrothermal method	GDY, $NiSO_4$, $FeSO_4$, urea, trisodium citrate	180 ℃, 12 h	Kuang et al. (2018)
Ni-Fe-LDH/GDY	Hydrothermal method	GDY, $Ni(NO_3)_2$, $Fe(NO_3)_3$, urea, trisodium citrate	150 ℃, 20 h	Si et al. (2019)
Mo^0/GDY	Hydrothermal method	GDY, Na_2MoO_4	120 ℃, 12 h	Hui et al. (2019c)
g-C_3N_4/GDY	Solvothermal method (N-methyl pyrrolidone, NMP)	GDY, g-C_3N_4	50 ℃, 10 h	Han et al. (2018)
CdS/GDY	Solvothermal method (dimethyl sulfoxide, DMSO)	GDY, $Cd(AcO)_2$, DMSO	180 ℃, 12 h	Lv et al. (2019)
WS_2/GDY	Solvothermal method (dimethyl formamide, DMF)	GDY, WCl_6, thioacetamide	120 ℃, 12 h	Yao et al. (2018)
CoN_x/GDY	GDY in-situ growth	CoN_x nanosheets, HEB, pyridine	110 ℃, 10 h	Fang et al. (2019)
Iron carbonate hydroxide/GDY	GDY in-situ growth	Iron carbonate hydroxide, HEB, pyridine	N_2, 60 ℃, 72 h	Hui et al. (2019a)
MoS_2/GDY	GDY in-situ growth	MoS_2 nanosheets, HEB, pyridine	Ar, 50 ℃, 15 h, in the dark	Hui et al. (2019b)
Ni^0/GDY	Electrochemical deposition	GDY, $NiSO_4$	10 mA cm^{-2}, 150 s	Xue et al. (2018)
Fe^0/GDY	Electrochemical deposition	GDY, $FeCl_3$	10 mA cm^{-2}, 250 s	Xue et al. (2018)
Ni-Fe-LDH/GDY	Electrochemical deposition	GDY, $Ni(NO_3)_2$, $FeSO_4$	−1.0 V vs SCE, 90 s	Shi et al. (2019)
Pd^0/GDY	Electrochemical deposition	GDY, $PdCl_2$	2 mA cm^{-2}, 10 s	Yu et al. (2019)
Ag/AgBr/GO/GDY	Oil-in-water microemulsion method	GO/GDY suspension, $AgNO_3$, cetyl trimethyl ammonium bromide (CTAB) in chloroform	Room temperature, adding oil to water dropwise within about 5 min	Zhang et al. (2015)
g-C_3N_4/GDY	Calcination method	GDY, g-C_3N_4	400 ℃, 2 h	Xu et al. (2019)
Co NPs wrapped by N-doped carbon/GDY	Sequential annealing treatments	GDY, $Co(AcO)_2$, dicyandiamide	1) Ar, 500 ℃, 2 h 2) Ar, 700 ℃, 2 h	Xue et al. (2016)
Pt NPs/GDY	Microwave-assisted reduction	GDY, chloroplatinic acid	400 W, 160 ℃, 2 min	Shen et al. (2019)

Table 2 A summary of the applications of GDY-supported catalysts.

Catalyst	Type of catalyst	Applications	Highlighted roles of GDY	Reference
TiO_2/GDY	Photocatalyst	Degradation of MB	(1) Decreasing the bandgap of TiO_2 (2) Extending the absorbable light range	Wang et al. (2012)
TiO_2/GDY	Photocatalyst	Degradation of MB	(1) Serving as an electron acceptor to improve the charge separation (2) Introducing abundant impurity levels (3) Improving the oxidation ability by lowering valance band positions	Yang et al. (2013)
ZnO/GDY	Photocatalyst	Degradation of MB, rhodamine B (RhB), and phenol	(1) Extending the absorbable light range (2) Serving as an electron acceptor to improve the charge separation	Thangavel et al. (2015)
Ag/AgBr/GO/GDY	Photocatalyst	Degradation of methyl orange (MO)	(1) Serving as an electron acceptor to improve the charge separation (2) Playing a synergistic role with GO	Zhang et al. (2015)
N-doped TiO_2/GDY	Photocatalyst	Degradation of RhB	Serving as an electron acceptor to improve the charge separation	Dong et al. (2018)
CdS/GDY	Photocatalyst	Hydrogen production via water splitting	(1) Serving as a hole acceptor to improve the charge separation (2) Stabilizing CdS NPs by preventing their agglomeration	Lv et al. (2019)
g-C_3N_4/GDY	Photocatalyst	Hydrogen production via water splitting	(1) Promoting charge separation and prolonging the charge carrier lifetime (2) Intensifying the electron density and decreasing the reaction overpotential (3) Facilitating electron mobility in the photocatalyst	Xu et al. (2019)
Co NPs wrapped by N-doped carbon/GDY	Electrocatalyst	Hydrogen production via water splitting	(1) Highly conductive support (2) Facilitating mass transfer by porous structure (3) Intensifying the electron density and improving the reaction activity (4) Protecting Co NPs from corrosion and aggregation (5) Providing more catalytic active sites	Xue et al. (2016)
$NiCo_2S_4$ nanowires/GDY	Electrocatalyst	Overall water splitting	(1) Serving as a highly conductive support for fast charge transfer (2) Improving the reaction kinetics by decreasing the charge transfer resistance and the contact resistance (3) Facilitating mass transfer and gas release by porous structure	Xue et al. (2017)
Ni-Fe-LDH/GDY	Electrocatalyst	Hydrogen production via water splitting	(1) Serving as a support for anchoring isolated single atoms (2) Improving the reaction kinetics by decreasing the charge transfer resistance and the contact resistance	Xue et al. (2018)

Catalyst	Type of catalyst	Applications	Highlighted roles of GDY	Reference
			(3) Protecting atomic catalysts from corrosion and aggregation	
WS_2/GDY	Electrocatalyst	Hydrogen production via water splitting	(1) Reducing reaction onset potential (2) Enhancing charge transfer in the hybrid catalyst (3) Protecting WS_2 from corrosion and agglomeration	Yao et al. (2018)
CoN_x/GDY	Electrocatalyst	Overall water splitting	(1) Serving as a highly conductive support for fast charge transfer (2) Facilitating mass transfer and gas release by porous structure (3) Improving the reaction kinetics by decreasing the charge transfer resistance and the contact resistance (4) Protecting CoN_x from corrosion	Fang et al. (2019)
Iron carbonate hydroxide/GDY	Electrocatalyst	Overall water splitting	(1) Providing more catalytic active sites by its large surface area (2) Improving the reaction kinetics by decreasing the charge transfer resistance and the contact resistance (3) Facilitating mass transfer and gas release by porous structure (4) Protecting Iron carbonate hydroxide from corrosion	Hui et al. (2019a)
MoS_2/GDY	Electrocatalyst	Hydrogen production via water splitting	(1) Serving as a highly conductive support for fast charge transfer (2) Improving the reaction kinetics by decreasing the charge transfer resistance and the contact resistance (3) Acting as an electron donor to enhance the metallic conductivity (4) Protecting MoS_2 from corrosion	Hui et al. (2019b)
Mo^0/GDY	Electrocatalyst	Ammonia and hydrogen production	(1) Improving the reaction kinetics by decreasing the charge transfer resistance and the contact resistance (2) Providing more catalytic active sites and enlarging electrochemical active surface area (3) Protecting Mo atoms from corrosion	Hui et al. (2019c)
Ni-Fe-LDH/GDY	Electrocatalyst	Overall water splitting	(1) Serving as a highly conductive support for fast charge transfer (2) Facilitating mass transfer and gas release by porous structure (3) Protecting Ni-Fe-LDH from corrosion	Si et al. (2019)
Pd^0/GDY	Electrocatalyst	Hydrogen production via water splitting	(1) Increasing the atomic efficiency and the number of active sites (2) Serving as a highly conductive support for fast charge transfer (3) Facilitating mass transfer and gas release by porous structure (4) Protecting Pd atoms from corrosion	Yu et al. (2019)